THE UNIVERSITY OF CALGARY

Electrorotation Measurements on Axolotl Embryos

by

Ghalia Abou-Ali

A THESIS

SUBMITTED TO THE FACULTY OF GRADUATE STUDIES

IN PARTIAL FULFILMENT OF THE REQUIREMENTS FOR THE

DEGREE OF MASTER OF SCIENCE

DEPARTMENT OF CHEMISTRY

CALGARY, ALBERTA

JANUARY, 2000

ABSTRACT

Electro-rotation is an established technique used to probe the frequency dependent electrical parameters of intact biological cells in suspension. This technique enables us to study the dynamics of ions and molecules inside the cell and its immediate vicinity, understand the associated polarization mechanisms as well as monitor the physiological state of cells such as fertilization.

This thesis describes the investigation of the frequency dependent dielectric properties of individual Xenopus and Axolotl (Ambystoma mexicanum) eggs utilizing the technique of electro-rotation. Individual amphibian eggs, immersed in a low conductivity media, were subjected to a known frequency and fixed amplitude rotating AC electric field and the resulting rotational motion of the embryo was monitored using a conventional optical microscope. None of the Xenopus embryos examined (stages 1 – 16) and the Axolotl embryos in the pre-gastrulation or neurulation stages of development exhibited any rotational motion over the field frequency range of 100 Hz to 2 MHz. However, the embryos in the gastrulation stages of development exhibited both co-field and counter-field rotation over different ranges of the applied field frequency. Typically the counter-field rotation exhibited a peak in the rotation spectra at ~5 kHz while the co-field peak was located at ~1.7 – 2 MHz. Using the simple shelled spherical model, the rotational spectral data were analyzed to determine the electrical parameters of Axolotl embryos during the early stages of development.

Although the shelled model was used to extract the electrical parameters our investigations show that such a model is not sufficient in explaining the temporal changes in the frequency dependent rotation spectrum. This thesis presents a new model that

includes a permanent dipole contribution to the torque, which does account for the lack of rotation at some particular stages of Axolotl development. The loss of rotation being due to a mutual cancellation of the torques generated by the permanent and induced dipoles.

ACKNOWLEDGEMENTS

At the beginning of this thesis, I would like to sincerely thank my supervisor, Dr. Reginald Paul, and co-supervisor, Dr. Karan Kaler, for their enlightening suggestions and valuable discussions throughout the research program. Their advice and encouragement are greatly appreciated. I also wish to express my deep gratitude to the examiners for their effort towards assessing this thesis. I am deeply grateful to Dr. Richard Gordon and Mrs. Natalie Bjorklund from University of Manitoba for providing the samples (Axolotl eggs) for experiments. Their profitable discussions, time and efforts in providing basic information about Axolotls including handling technique instructions are greatly appreciated. Dr. Sarah McFarlane generously supplied us with Xenopus embryos for experiment; I thank her and her group for their kind assistance. I very much thank my husband, Mustapha Moussa, for his moral support and his assistance in the mechanics of preparing this thesis.

Finally, I wish to acknowledge the financial support from the Faculty of Graduate Studies and the Department of Chemistry through Graduate Research and Teaching Assistantship. This research was supported by the NSERC (Natural Science and Engineering Research Council of Canada) grants to Dr. R. Paul and K.V.I.S. Kaler.

To

my mother,

Nabiha Hammoud

TABLE OF CONTENTS

LIST OF TABLES

LIST OF FIGURES

LIST OF SYMBOLS

Abbreviations:

ROT	Electro-rotation
rms	root mean square
Vpp	peak-to-peak voltage

Operators:

∇	gradient operator
Im[...]	imaginary part
Re[...]	real part

Symbols:

α,θ,γ	polar angles from z-axis
β,ϕ,φ	azimuthal angles
δ	angle between externally applied electric field and permanent dipole vector
χ	phase angle
η	medium viscosity
ω	radian field frequency
f	field frequency
L	number of counterions per unit area

$\bar{T}_{ROT}$	rotational torque exerted on a simple sphere
T_f	frictional force
S	particle rotational velocity
$\bar{E}_{ROT}$	rotating electric field vector
E_0	electric field strength
r	radius of a spherical particle
R	radius of a shelled spherical particle (embryo)
d	shell thickness
D	diffusion coefficient of ions
a	inner radius of one-shelled spherical particle
b	outer radius of one-shelled spherical particle
$\bar{P}_{per}$	net permanent dipole moment
$\bar{P}_{ind}$	field-induced dipole moment of a particle
$\bar{P}$	total dipole moment of a particle
$\bar{\mu}_{eff}$	induced effective dipole moment of a particle
M	permanent dipole moment magnitude
Y_{nm}	spherical harmonics
P_n^m	associated Legendre polynomial
Ψ	electric potential
$\underline{K}$	Clausius-Mossotti factor
Z	quotient of particles radius and Debye screening

	length
υ	volume fraction of the particles
ε_p	particle permittivity
ε_m	medium permittivity
ε_∞	permittivity at infinite frequency
ε_s	permittivity at low frequency
ε_0	permittivity of free space
ε_r	relative permittivity
ε_{in}	permittivity of the inside of a shelled-particle
ε_{sh}	permittivity of the shell of a particle
ε_{eff}	effective permittivity
ε_{pm}	effective permittivity for simple shelled particle
ε'	real part of the complex permittivity
ε''	imaginary part of the complex permittivity
ε^*	complex permittivity
ε_m^*	complex permittivity of medium
ε_p^*	complex permittivity of particle
ε_{eff}^*	effective complex permittivity
ε_{sh}^*	complex permittivity of the shell
σ_p	particle conductivity
σ_m	medium conductivity

σ_{sh}	conductivity of the shell
σ_{eff}	effective conductivity
σ_{pm}	effective conductivity for simple shelled particle
σ_{in}	conductivity of the inside of a shelled-particle
σ_{p}^{*}	complex conductivity of the particle
σ_{m}^{*}	complex conductivity of the particle
σ_{eff}^{*}	effective complex conductivity
Y_{surf}^{*}	surface admittance
G_{sh}	shell conductance
G_{surf}	surface conductance
C_{sh}	shell capacitance
C_{surf}	surface capacitance
τ	relaxation time constant
τ_{MW}	Maxwell-Wagner relaxation time constant
τ_{α}	relaxation time at low frequency
τ_{β}	relaxation time at high frequency
τ_{LF}	time constant of low frequency relaxation

CHAPTER 1

INTRODUCTION

1.1 Properties of Biological Particles and Applications

The study of the electric and dielectric properties of biological particles is a crucial and active area of research because of their important applications in several areas including biophysics, biotechnology, physiology and medical engineering. Measurements of the electrical parameters of cells can be used to determine the effects of chemical agents and various drugs on living cells. Such measurements can also be utilized to sort cells [1-2] and distinguish diseased cells from healthy cells [2-4]. Furthermore, the determination of dielectric properties has potential applications in measuring the concentration of biological products such as soybean phosphatide [5]. Other applications of studies concerning dielectric properties are the determination of diffusion coefficients of proteins in solution, the study of radio-frequency of electric fields emitted by living cells [6], and cell manipulations [7].

1.2 Electrical Measurement Methods

A variety of techniques have been employed to study the electrical properties and dielectric response of biological particles. Such studies provide information about cell membranes, the dynamics of ions inside the cells, and allow us to understand the polarization mechanism(s) associated with biological particles under different conditions. The most common physical methods used for studying the characteristics of biological cells are the suspension method [8-9], the micropipette method [10], electrophoresis [11], dielectrophoresis [12-13] and electro-rotation [14] methods. This thesis examines only

electro-rotation as it is applied to a complicated biological system. In order to understand this work well, electro-rotation will be briefly discussed at this point.

Electro-rotation (ROT) is the motion due to a rotational torque exerted on a polarized particle under the influence of a rotating AC electric field [14]. This non-invasive technique has wide applications in cell separation [15], determining membrane properties such as capacitance per unit area for a variety of cells including plant protoplast [14], plant cell vacuoles [16] and oocytes [17]. A considerable amount of work, both practical and theoretical, has been published since Arnold and Zimmermann [14] reported that single cells were found to rotate in a rotating electric field in 1982. Sauer [18] has shown that the electrical torque is related to the imaginary part of the excess effective polarizability $\underline{K}$ (shown in Equation 2.4 below). An electro-rotation spectrum can be obtained by measuring the particle rotational velocity (which is related to the torque) as a function of the frequency of the externally applied electric field. By fitting the experimental rotational spectrum to a suitable theoretical model, dielectric properties such as membrane capacitance/ conductance can be extracted.

1.3 Thesis Objectives

As mentioned earlier, electro-rotation technique has been used to probe the frequency dependent electrical properties, i.e., conductivity and permittivity of intact biological cells. Electro-rotational measurements have also proven a sensitive method for monitoring the physiological state of cells such as fertilization and cell fusion. For instance, Muller et. al. [19] studied the properties of mouse oocytes and measured the electric parameters of cell components. In another study, the differences in membrane

properties between unfertilized and fertilized rabbit oocytes were demonstrated by electro-rotation [17]. It was found that the apparent membrane capacity of rabbit oocytes increased upon fertilization. In addition, the membrane conductivity and capacitance of cells obtained from 2-, 4-, or 8-cell embryos were measured [17]. As the examples above show, electro-rotation technique has been limited in its application to simple systems such as single cells or oocytes. In this work, the Axolotl embryo is used as a model for a multi-cellular system so that the applicability of electro-rotation technique to complicated systems can be tested.

It has been suggested that the ionic currents and voltage gradients, detected and measured by Metcalf and co-workers [20], might constitute factors that control the embryonic development in Axolotls. However, the precise mechanisms by which the above-mentioned electrical phenomena operate are still unknown and a knowledge of the basic electrical properties (permittivities and conductivities) of the embryos is desirable. Knowledge of electrical properties might help in understanding the development of these embryos. It is the aim of this thesis to use the method of electro-rotation for measuring and quantifying, with simple models, such essential information during the early stages of embryogenesis.

Expressions for the rotational torque acting on spheres of different structures, starting with homogenous dielectric sphere and building up to multi-shelled bodies have already been developed. However, in all the extant theoretical work in this field, only a dipole moment induced by the applied field has been thus far considered, neglecting any contributions from permanent polarization that might be present. In this thesis, the electro-rotation conventional theory that is based on an induced dipole approach is

extended to include a permanent dipole moment contribution since many particles might possess a permanent dipole.

1.4 Thesis Outline

Chapter 2 is a brief review of the basic conventional theory of electro-rotation including the discussion of relevant polarization mechanisms and typical models. In chapter 3, the experimental set-up is shown, followed by the preparation of samples. Experimental results (rotation spectra) are shown and discussed in chapter 4 where electrical parameters are calculated by fitting the results to the one-shelled model. In addition, a theoretical model, based on the permanent dipole moment approach is presented in chapter 5. Chapter 6 includes some conclusions and recommendations for possible future work. Basic information regarding the Axolotl embryos is given in appendix A, which shows the series of developmental-stages adopted in this work.

CHAPTER 2

LITERATURE REVIEW

2.1 Historical Background on Particle Rotation

Starting in 1896 Quincke [21] discovered that an intense electrostatic field would cause a dielectric body immersed in a non-conducting medium to rotate (Quincke rotation). At the end of last century, several laboratories used rotating fields for the measurement of the dielectric properties of macroscopic bodies. It was demonstrated at that time that a rotating field can induce a torque in a stationary dielectric body. These experiments prompted the development of an early theory in an attempt to explain/interpret the rotation field measurements. The first calculation, carried out by Lampa [22] in 1906, was done for the case of two dielectrics (a sphere and the surrounding medium) placed in a rotating electric field. No membrane or other dielectric layer was included in the calculations. From the polarization and conduction components of the current the surface charge density on the interface of the two dielectrics can be calculated through the magnetically caused current. The torque in this case is the consequence of the interactions between the surface charges and the applied field. In this early work Lampa demonstrated that a homogenous sphere of radius r in a rotating field of strength E_0 experiences a torque T which depends on the radian field frequency ω and is given by the following equation:

$$T = 12\pi\varepsilon_p E_0^2 r^3 \omega \frac{\varepsilon_p\sigma_m - \varepsilon_m\sigma_p}{(\sigma_m + 2\sigma_p)^2 + \omega^2(\varepsilon_m + 2\varepsilon_p)^2} \qquad (2.1)$$

The symbols ε and σ represent the permittivity and conductivity respectively. The subscript m and p stand for medium and particle.

As interest in the application of electric fields to living cells increased in the 1960's, Texieira-Pinto et al reported [23] that living cells may rotate when subjected to an alternating (non-rotating) field. Following this, Pohl [1-2] found that yeast cells could be made to rotate anywhere in the field between electrodes. In 1981, the phenomenon of multi-cell rotation in an alternating electric field was discovered [24] and this led to the prediction that a single cell should spin in a rotating electric field. Indeed, Arnold and Zimmermann [14] reported a single cell rotation in a rotating field first in 1982. Since then, the rotation of cells in rotating fields, which was later named as "electro-rotation", was further experimentally investigated by Arnold and Zimmermann [25-28], Fuhr [15, 29-30, 19, 31], Glaser [16, 32], Kaler [33-34], Pethig [35-36] and other researchers [37-38]. They have experimentally improved several aspects of this technique including design of measuring chamber, generation of rotating fields and detection of cell rotating velocity. In these studies, investigations on different types of particles have been carried out. These investigations include protoplasts, mammalian oocytes, yeast cells, latex particles, swollen thylakoid vesicles and much more.

The above-mentioned observed cell rotation, induced by external electric field at various frequencies, gave rise to much theoretical analysis, which lead to an evaluation of the electrical cell properties. Holzapfel et al [39] introduced a dipole-dipole interaction theoretical interpretation for the multi-cell rotation observed in high suspension densities of yeast, plant protoplasts and mammalian cells [40]. He assumed that the rotation in a linear alternating electric field arises from the interaction of electrically induced dipole

moments in adjacent cells. Based on same theory, an equation for the rotation of single cells in a planar homogenous rotating field was derived [14], with the polarization mechanism being both the charge separation across the membrane and the interaction of the rotating field with an induced cellular dipole. It is indicated that the charging of the membrane produced the dipole. The charging time (τ) of a thin spherical membrane exposed to an external electric field was given by Schwan [8] and by Jeltsch and Zimmermann [41]. Since most biological particles are multi-layer systems, Fuhr [29-30] developed a model for multi-layer spherical cells.

The early theory [18] based on the principle of momentum conservation enables us to calculate torques exerted on bodies of simple shape such as cylinders and spheres with a shell structure using the Maxwell's stress tensor approach. From this, the torque can be obtained by taking a vector cross product with the radius vector followed by an integration over the entire surface of the cell. This method is hard to work with since the computation of surface integral might be difficult to obtain for certain geometrical shapes of the cell. As a result, much of the work carried out in this field employed calculating an effective dipole moment induced on the cell by the external field first, and then computing the torque exerted on this latter using the standard formulae from classical mechanics. Turcu and Lucaciu [42] proposed a unitary approach to all electro-rotation phenomena in 1989. They analyzed the electro-rotation torque acting on a simple spherical object and on a spherical object surrounded by a single shell, giving the complete algebraic expression and some systematic approximations.

In a simple cell model, the cell surface is assumed electrically neutral. But, in reality, the cell surface is charged and thus acquires a layer of counter ions referred to as

the double layer. One of the earliest attempts on charged spherical particles was made by O'Konski [43] who derived an expression for the surface conductance. In later work, Schwarz [44] explained a surface diffusion process to accompany the electrically driven motion of the ions and surface conductance. In order to account for the coupling of the tangential surface flux with bulk medium, Dukhin and Shilov [45] developed a new approach based on the concept of the diffuse double layer.

In the above-mentioned surface conductance models of biological particles, the approaches assume that the charges are smoothly distributed on the surface of the particle. In reality the surfaces of these particles are not smooth but are characterized by the presence of regions of high and low charge densities. As a consequence, Paul [46] introduced a new model in which he presented a more realistic description of the counter ion motion. He described that an ion would become trapped in a high charge density region and its ability to follow an externally applied electric field would depend upon the time afforded by the latter to the ion to escape from the trap. This situation would result in a frequency-dependent surface conductance.

At this point, it is appropriate to introduce the conventional electro-rotation theory, as it is known today. Fundamental features and equations associated with this theory are presented next.

2.2 Basic Theory of Electro-rotation

Electro-rotation technique has been used to study the electrical properties of biological particles. The phenomenon of electro-rotation occurs as a result of the rotational torque exerted on a polarizable dielectric particle by a rotating electric field.

The rotational torque ($\bar{T}_{ROT}$) is related to the particle properties as follows [3, 14]:

$$\bar{T}_{ROT} = \bar{\mu}_{eff} \times \bar{E}_{ROT} \tag{2.2}$$

where $\bar{\mu}_{eff}$ is the induced effective dipole moment of the particle and $\bar{E}_{ROT}$ is the rotating electric field vector.

For a spherical particle of radius r, which has no permanent dipole moment, placed in an external field, the time average torque $< \bar{T}_{ROT} >$ is:

$$< \bar{T}_{ROT} >= -4\pi\varepsilon_m r^3 \, \mathrm{Im}[\underline{K}] E_0^2 \hat{z} \tag{2.3}$$

where E_0 is the electric field strength and $\underline{K}$ is the Clausius-Mossotti ratio, which represents the frequency-dependent effective polarizability and can be expressed as:

$$\underline{K} = \frac{\varepsilon_p^* - \varepsilon_m^*}{\varepsilon_p^* + 2\varepsilon_m^*} = \frac{\sigma_p^* - \sigma_m^*}{\sigma_p^* + 2\sigma_m^*} \tag{2.4}$$

ε^* and σ^* are the complex permittivity and conductivity defined as:

$$\varepsilon^* = \varepsilon - j\frac{\sigma}{\omega} \tag{2.5}$$

$$\sigma^* = \sigma + j\omega\varepsilon \tag{2.6}$$

The subscript p and m refer to the particle and medium respectively. ω is the electrical frequency in radians per second and $j = \sqrt{-1}$

At a constant cell rotational velocity (S), the rotational torque T_{ROT} is balanced by the oppositely directed torque arising from the frictional force T_f [39], given by

$$T_f = -8\pi\eta \, Sr^3 \tag{2.7}$$

where r is the cell radius and η is the viscosity of the medium. At equilibrium,

$$T_{ROT} + T_f = 0 \tag{2.8}$$

Combining Equation (2.3), (2.7) and (2.8), the cell rotational velocity is obtained:

$$S = -\frac{\varepsilon_m}{2\eta} \mathrm{Im}[\underline{K}] E_0^2 \tag{2.9}$$

Equation (2.9) shows that the cell rotational velocity (S) is proportional to the square of field strength. Rotation velocity is also proportional to the Im[$\underline{K}$], and therefore, the cell polarization ROT spectrum (Im[$\underline{K}$] vs. field frequency f) obtained from experimental rotation spectrum (rotation velocity S vs. field frequency f) can be used to study the electrical properties of biological cells.

There are several known modes of polarization in matter. There include electronic, atomic, dipolar, interfacial and counterion polarization. All polarization mechanisms are dependent on the frequency of the applied field; some operate at only low frequency while others might be evident only at high frequencies. In this chapter, three polarization mechanisms that mainly give biological cells their dielectric properties will be reviewed. The mechanisms include dipolar orientation, interfacial polarization and ionic diffusion.

2.3 Dipolar Polarization (Debye Polarization)

This polarization mechanism arises from the orientational responses of molecules or parts of molecule [4]. As shown by Debye, molecules may posses permanent dipoles and these dipoles tend to respond to an external field by realignment in order to reduce their potential energy. However, when the frequency of the field is high, the molecules cannot change direction fast enough to follow the field and make no contribution to the polarization of the sample [47].

The dielectric response of a material in an electric field involves the physical displacement of charge. At high field frequency, the induced dipole can no longer keep up with the charging field, and as a result, a relaxation process can be observed in the form of polarization dispersion. Relaxation effects can be usually described by first order differential equations that yield a single time constant. A simple case where the dipolar polarization of a sample will relax towards the steady state by relaxation time τ, can be described by the following expressions:

$$\varepsilon^* = \varepsilon_\infty + \frac{(\varepsilon_s - \varepsilon_\infty)}{1 + j\omega\tau} \tag{2.10}$$

$$\varepsilon^* = \varepsilon' - j\varepsilon'' \tag{2.11}$$

ε^* is the complex permittivity, $\varepsilon^* = \varepsilon_r \times \varepsilon_0$, ε_r is the relative permittivity and ε_0 is the permittivity of free space. ε_∞ and ε_s are the permittivity at infinite frequency (electronic polarization) and low frequency (static) respectively. Also, ε' and ε'' are the real and imaginary parts of the complex permittivity:

$$\varepsilon' = \varepsilon_\infty + \frac{(\varepsilon_s - \varepsilon_\infty)}{1 + (\omega\tau)^2}, \qquad \varepsilon'' = \frac{(\varepsilon_s - \varepsilon_\infty)\omega\tau}{1 + (\omega\tau)^2} \tag{2.12}$$

The time scale and the exact shape of relaxation are related to the structure of the material. If the polarization is caused by the orientation of small molecules then the relaxation process may take about 10^{-11} s (example, some liquids), whereas if the polarization is caused by the orientation of large polar molecules (example, proteins in aqueous solution), the relaxation time is in the order of $10^{-8} - 10^{-6}$ s [48].

2.4 Interfacial Polarization (Maxwell-Wagner)

Interfacial polarization arises from the charge accumulation at the interfaces of heterogeneous materials. Charge accumulations are caused by the migration of charged carriers through the several phases of the dielectric [4]. When these charges or carriers are hindered in various ways, this hindrance of their motion appears to the experimenter as polarization. This polarization mechanism can also be seen as a result of the boundary conditions on the fields at the interfaces between the different phases. The characteristic time constant for this mechanism, τ_{MW}, can be realized by recasting Equation (2.4) in the following form:

$$\underline{K} = \frac{\sigma_p - \sigma_m}{\sigma_p + 2\sigma_m}\left[\frac{j\omega\tau_0 + 1}{j\omega\tau_{MW} + 1}\right] \tag{2.13}$$

where $\tau_0 \equiv \frac{\varepsilon_p - \varepsilon_m}{\sigma_p - \sigma_m}$ and $\tau_{MW} \equiv \frac{\varepsilon_p + 2\varepsilon_m}{\sigma_p + 2\sigma_m}$. This expression shows Maxwell-Wagner polarization as a dispersive response of a homogenous ohmic dielectric sphere immersed in an ohmic dielectric medium. Several models have been developed to study the dielectric properties of biological cells and tissues. In this section, the dielectric properties of a few simple models representing biological particles will be discussed.

2.4.1 The Homogenous Spherical Model

Consider a homogenous biological particle of radius r, permittivity ε_p and conductivity σ_p, immersed in a medium of dielectric properties ε_m and σ_m. By

substitution of Equation (2.5) into Equation (2.4), followed by expansion by partial fractions, $\underline{K}$ can be expressed as [49]

$$\underline{K} = \frac{\Delta K}{(1 + j\omega\tau)} + K_{\infty} \tag{2.14}$$

where

$$\Delta K = \frac{3(\varepsilon_m \sigma_p - \varepsilon_p \sigma_m)}{(\varepsilon_p + 2\varepsilon_m)(\sigma_p + 2\varepsilon_m)} \tag{2.15}$$

$$K_{\infty} = \frac{(\varepsilon_p - \varepsilon_m)}{(\varepsilon_p + 2\varepsilon_m)} \tag{2.16}$$

Thus, $\underline{K}$ shows a single relaxation at relaxation time τ

$$\tau_{MW} = \frac{(2\varepsilon_m + \varepsilon_p)}{(2\sigma_m + \sigma_p)} \tag{2.17}$$

This relaxation (Maxwell-Wagner), which is associated with the charging of the interface between two phases due to differences in their bulk electrical properties, occurs even if the dielectric properties of the individual phases are independent of frequency. The real and imaginary parts of $\underline{K}$ are

$$\mathrm{Re}[\underline{K}] = \frac{\Delta K}{1 + (\omega\tau)^2} + K_{\infty} \tag{2.18}$$

$$\mathrm{Im}[\underline{K}] = \frac{-\Delta K \omega\tau}{1 + (\omega\tau)^2} \tag{2.19}$$

The frequency regime to which this type of mechanism (Maxwell-Wagner) is applicable can be determined by examining both the low and high frequency limits in the Clausius-Mossotti expression in Equation (2.4) resulting in:

$$(\sigma_p - \sigma_m)/(\sigma_p + 2\sigma_m) \qquad \text{(low frequency)} \tag{2.20}$$

$$(\varepsilon_p - \varepsilon_m)/(\varepsilon_p + 2\varepsilon_m) \qquad \text{(high frequency)} \qquad (2.21)$$

The point of transition between the two limits is at $1/\tau$. In contrast, Im[$\underline{K}$] has a broad peak of amplitude $\Delta K / 2$ that may be positive or negative. Fig. 2.1 shows an example of frequency dependence of the real and imaginary parts of the complex susceptibility for the spherical model. In the ROT spectrum (Imaginary part), when Im[$\underline{K}$] >0, counter-field rotation arises, i.e., particles rotate against the field. This counter-field rotation occurs when the field induced dipole moment $\bar{\mu}$ leads $\bar{E}_{ROT}$ by an angle ranging from 0^0 to 180^0. While co-field rotation occurs when $\bar{\mu}$ lags behind $\bar{E}_{ROT}$ by 0^0 to 180^0 (Im[$\underline{K}$] < 0).

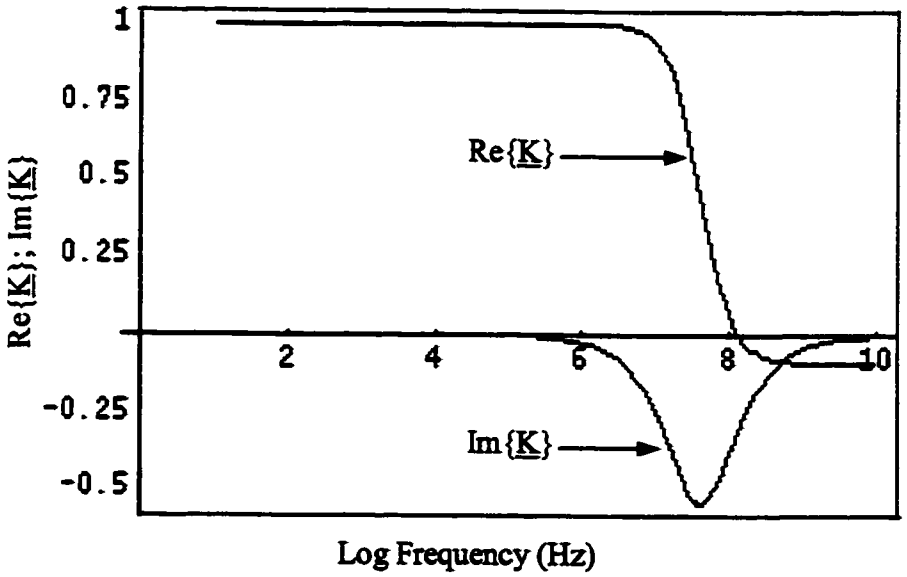

Fig.2.1 Real and Imaginary parts of $\underline{K}$ of a homogenous spherical particle: σ_p =5000μS/cm, σ_m = 10 μS/cm, $\varepsilon_p = 60\varepsilon_0$, $\varepsilon_m = 80\varepsilon_0$, r=17.5 μm

2.4.2 The Simple-Shelled Spherical Model

It is known that biological cells have membranes of about 5 nm in thickness. The cell membrane is mainly composed of a bilayer of long-chain lipid molecules, which normally have very low conductivity. The interior of biological cells, the cytoplasm is highly conductive and may be well approximated by a conducting homogenous medium. Biological cells and more complex biological systems can be represented by more complicated model systems that exhibit multiple dispersion. Simple- and multi-shelled spheres (for modeling cells with intracellular organelles) were studied by many workers in both fields of dielectrophoresis and electro-rotation [42, 29, 12, 32,and 50]. In such complicated systems, $\underline{K}$ exhibits several dispersions that are equal to the number of different interfaces in the system. In this section, the discussion will be limited to the simple-shelled (one shell) sphere case.

Maxwell-Wagner theory can be extended to discuss a sphere surrounded by a thin shell of thickness d and dielectric properties ε_{sh} and σ_{sh} (see Fig.2.2). The dielectric response of such particle can be represented by an equivalent homogenous sphere of complex permittivity ε^*_{eff}

$$\varepsilon^*_{eff} = \varepsilon_p \frac{u^3 + 2\underline{K}(\varepsilon^*_p, \varepsilon^*_{sh})}{u^3 - \underline{K}(\varepsilon^*_p, \varepsilon^*_{sh})} \tag{2.22}$$

where

$$\varepsilon^*_{sh} = \varepsilon_{sh} - j\frac{\sigma_{sh}}{\omega} \tag{2.23}$$

$$u = \frac{r + d}{r} \tag{2.24}$$

and $\underline{K}$ is the same complex effective polarizability defined in Equation (2.4) with the medium replaced by the shell. The new Clausius-Mossotti factor $\underline{K}$ to be included in the torque expression (in Equation (2.3)) is given by

$$\underline{K}(\varepsilon_{eff}^*, \varepsilon_m^*) = \frac{\varepsilon_{eff}^* - \varepsilon_m^*}{\varepsilon_{eff}^* + 2\varepsilon_m^*} \tag{2.25}$$

Inserting the quantities $\varepsilon_m, \sigma_m, \varepsilon_{sh}, \sigma_{sh}, \varepsilon_p, \sigma_p$, r and d into Equation (2.25), it becomes

$$\underline{K} = \frac{\omega^2(\tau_m\tau_{sh} - \tau_p\tau'_{sh}) - 1 + j\omega(\tau'_{sh} - \tau_m - \tau_m)}{2 - \omega^2(\tau_p\tau'_{sh} + 2\tau_m\tau_{sh}) + j\omega(\tau'_{sh} + 2\tau_m + 2\tau_{sh})} \tag{2.26}$$

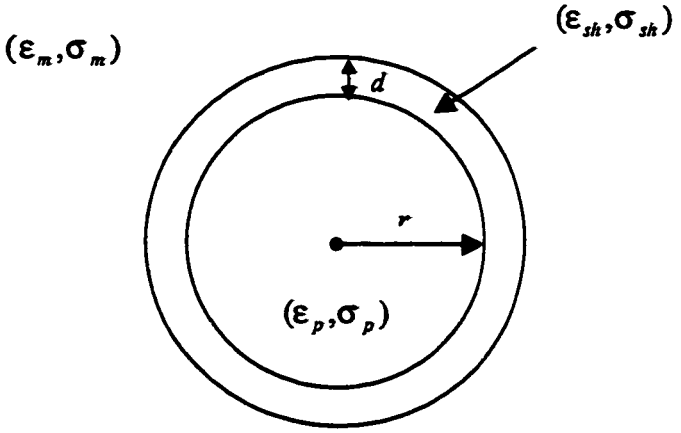

Fig.2.2 Simple shelled model for biological cells in an ohmic medium.

$$\tau_p = \varepsilon_p / \sigma_p \tag{2.27}$$

$$\tau_{sh} = c_{sh} r / \sigma_p \tag{2.28}$$

$$\tau_m = \varepsilon_m / \sigma_m \tag{2.29}$$

$$\tau'_{sh} = c_{sh} r / \sigma_{eff} \tag{2.30}$$

Equation (2.26) looks quite complicated, and therefore, it is difficult to determine the direct contribution of each of the parameters to the frequency-dependent Im[$\underline{K}$], i.e. The rotational spectrum. In order to estimate /discuss the contribution of each parameter to rotation, a series of ROT spectra were plotted. For each group of curves, shown in Fig.2.3, only one parameter was varied, while others were kept constant and assigned reasonable values in terms of biological cells particularly plant protoplast in this case.

Fig.2.3B—Fig.2.3F show that particle radius, medium conductivity, and membrane capacitance have effects on the low-frequency (100 Hz to 100 kHz) relaxation, whereas both particle permittivity and conductivity affect the high frequency relaxation (> 1 MHz). The simple shelled model predicts no relaxation at very low frequencies (< 100 Hz).

The two polarization relaxations predicted in the theoretical ROT spectra can be physically interpreted as follow: above field frequency of 20 kHz, the membrane appears transparent to the externally applied field, therefore the field sees a homogenous conductive sphere immersed in a medium. Hence, in this case the ROT spectrum is controlled by σ_p and σ_m (see Equation 2.20) and the relaxation time is given by Equation 2.17. The peak above 1 MHz is controlled by ε_p and ε_m (see Equation 2.21). At frequency of 300 Hz and below, the field is unable to penetrate the cell membrane, hence the particle behaves like an insulating system.

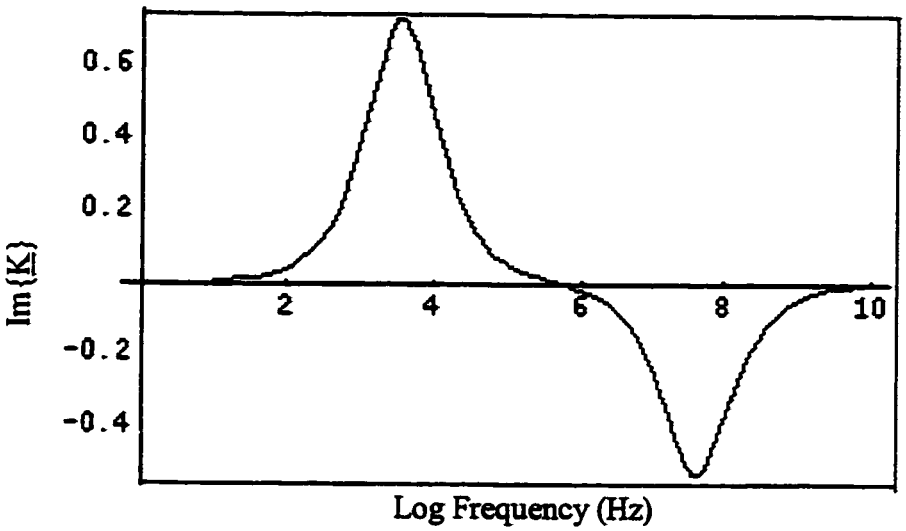

Fig.2.3A Typical theoretical ROT spectrum for the simple shelled sphere model, $\varepsilon_m = 80\varepsilon_0$, $\varepsilon_p = 60\varepsilon_0$, $C_{sh} = (\varepsilon_{sh}/d) = 0.5$ μF/cm^2, $\sigma_m = 10$ μS/cm, $\sigma_p = 5000$ μS/cm, $\sigma_{sh} = 0.0$ μS/cm, $r = 17.5$ μm.

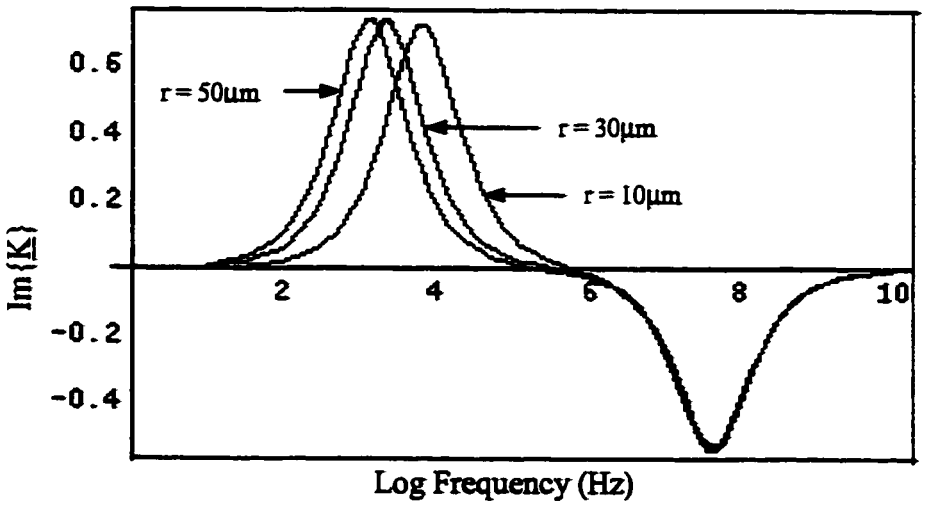

Fig. 2.3B Radius dependence of ROT spectrum for the shelled spherical model, $\varepsilon_m = 80\varepsilon_0$, $\varepsilon_p = 60\varepsilon_0$, $C_{sh} = 0.5$ μF/cm^2, $\sigma_m = 10$ μS/cm, $\sigma_p = 5000$ μS/cm, $\sigma_{sh} = 0.0$ μS/cm.

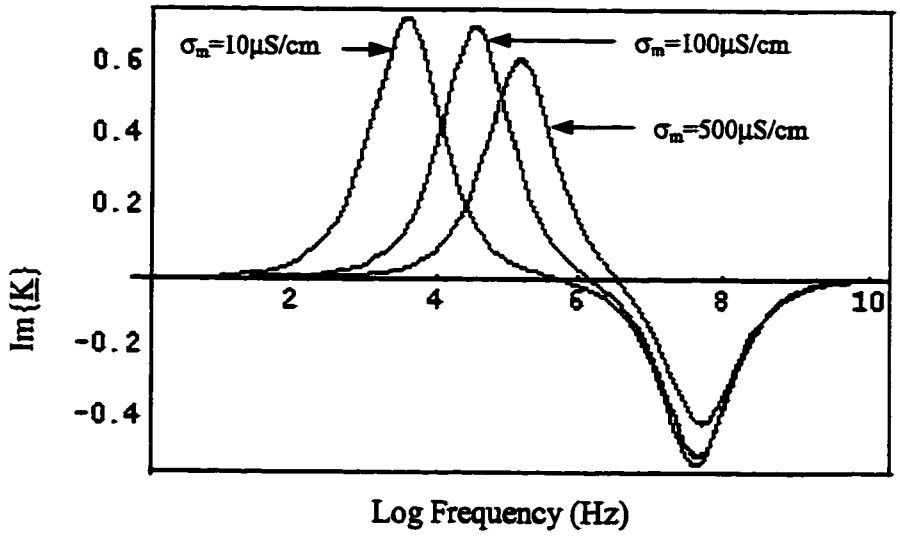

Fig.2.3C σ_m dependence of ROT spectrum for the shelled spherical model,

$\varepsilon_m = 80\varepsilon_0$, $\varepsilon_p = 60\varepsilon_0$, $C_{sh} = 0.5$ μF/cm^2, $\sigma_p = 5000$ μS/cm, $\sigma_{sh} = 0.0$ μS/cm, $r = 17.5$

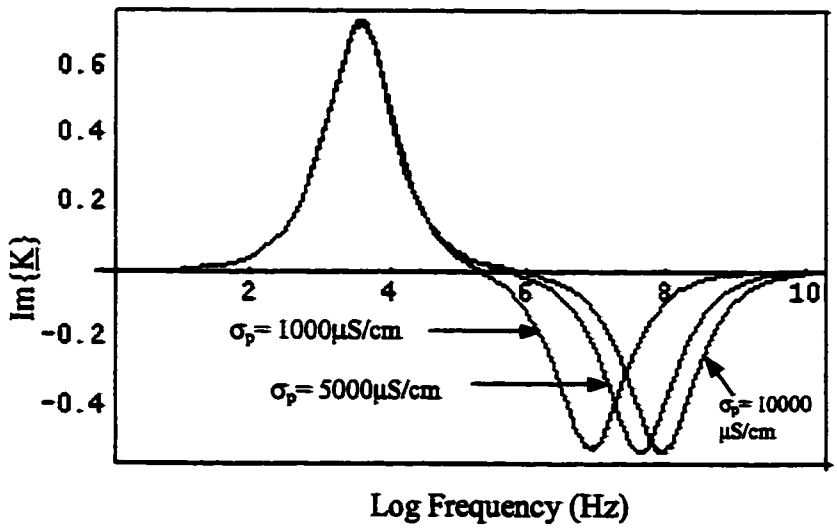

Fig.2.3D σ_p dependence of ROT spectrum for the shelled spherical model,

$\varepsilon_m = 80\varepsilon_0$, $\varepsilon_p = 60\varepsilon_0$, $C_{sh} = 0.5$ μF/cm^2, $\sigma_m = 10$ μS/cm, $\sigma_{sh} = 0.0$ μS/cm, $r = 17.5$ μm

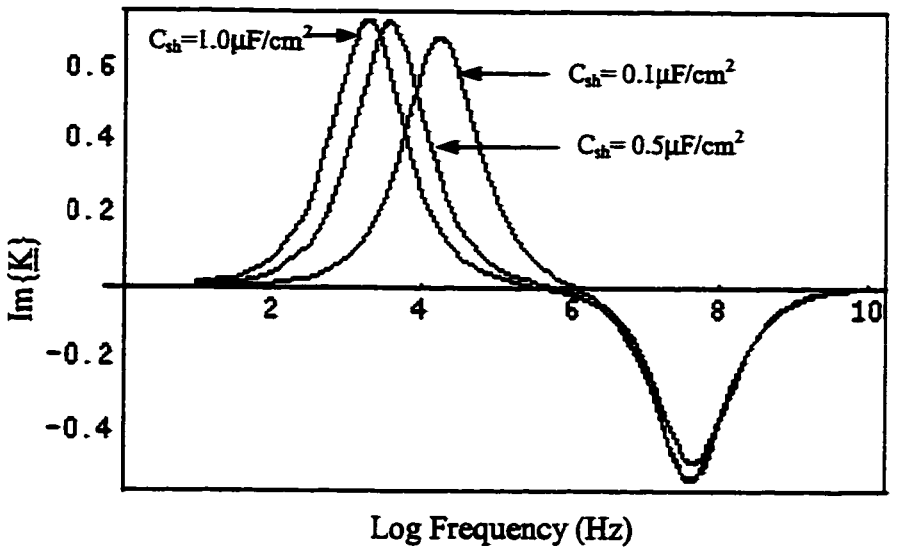

Fig.2.3E C_{sh} dependence of ROT spectrum for the shelled spherical model, $\varepsilon_m = 80\varepsilon_0$, $\varepsilon_p = 60\varepsilon_0$, $\sigma_m = 10$ μS/cm, $\sigma_p = 5000$ μS/cm, $\sigma_{sh} = 0.0$ μS/cm, $r = 17.5$ μm.

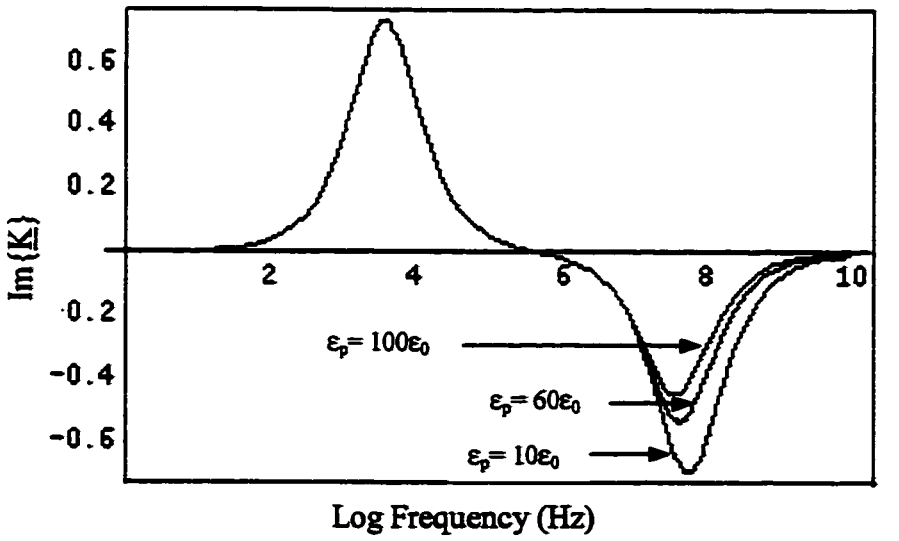

Fig.2.3F ε_p dependence of ROT spectrum for the shelled spherical model, $\varepsilon_m = 80\varepsilon_0$, C_{sh}=0.5 μF/cm^2, $\sigma_m = 10$ μS/cm, $\sigma_p = 5000$ μS/cm, $\sigma_{sh} =$ 0.0 μS/cm, $r = 17.5$ μm.

2.4.3 The Shell with Surface Admittance Model

Typically, cell membranes have a high surface charge density, and a correspondingly high and possibly frequency-dependent surface admittance. Thus, the rotational spectra might exhibit dispersions associated with the surface admittance in addition to charging of the membrane capacitance [49].

The case of a nonconductive particle surrounded by a shell with a complex admittance was discussed by Schwan [49], and (for frequency-independent surface conductance) by Chizmadzhev [51]. To discuss the case of a particle with surface admittance [49], let ε_{in} and σ_{in} represent the dielectric properties of the particle interior, and C_{surf} and G_{surf} are the surface capacitance and conductance respectively. The complex effective particle conductivity is

$$\sigma^*_{eff} = \sigma^*_{in} + 2\sigma^*_{sh}\frac{d}{r} = \sigma^*_{in} + 2\frac{Y^*_{surf}}{r} \tag{2.31}$$

where

$$Y^*_{surf} = G_{surf} + j\omega C_{surf} \tag{2.32}$$

Y^*_{surf} is the surface admittance. d and σ^*_{sh} are the thickness and the complex conductivity of the shell respectively (as defined for the simple-shelled model in section 2.4.2). The effective dielectric properties of the particle are then

$$\sigma_{eff} = \sigma_{in} + 2\frac{G_{surf}}{r} \tag{2.33}$$

$$\varepsilon_{eff} = \varepsilon_{in} + 2\frac{C_{surf}}{r} \tag{2.34}$$

Therefore the Classius-Mossoti factor becomes

$$\underline{K}(\varepsilon^*_{eff}, \varepsilon^*_m) = \frac{\varepsilon^*_{eff} - \varepsilon^*_m}{\varepsilon^*_{eff} + 2\varepsilon^*_m} \tag{2.35}$$

where

$$\varepsilon^*_{eff} = \varepsilon_{eff} - \frac{\sigma_{eff}}{j\omega} \tag{2.36}$$

$$\varepsilon^*_m = \varepsilon_m - \frac{\sigma_m}{j\omega} \tag{2.37}$$

In a ROT spectrum, it is expected that a decrease in the cell surface capacitance will cause the low-frequency (~100 Hz to 100kHz) dispersion peak to move towards high frequency with almost the same amplitude. With decreasing the surface conductance, this peak will also shift towards higher frequency but the amplitude would diminish. In addition, theoretical predictions reveal that surface capacitance should play an important role in high frequency (> 100 kHz) relaxation, while surface conductance has no effect on this high frequency relaxation.

2.5 Counterion Polarization

Counterion polarization is a result of ionic diffusion within the electrical double layer that consists of a layer of counterions, which encompass the surface charge ions in a spherically symmetric fashion. When an external electric field is applied, the symmetry of the counterionic cloud will be broken resulting in an induced polarization. Counterion effects have been observed in different systems including emulsions, charged polystyrene sphere suspensions, and linear macromolecules including DNA [52]. The effects of this type of polarization are large at low frequencies and contribute to the α-dispersion observed in tissues at low frequency. Many theoretical models have been proposed to

describe and explain the counterion effects. The bound-ion layer was first proposed by Schwarz [44] to explain the low frequency dielectric dispersion observed with colloidal particles suspended in electrolyte solution. In his work, Schwarz successfully described the amplitude of the dispersion. Schurr [53] extended this ion-bound theory to include tangential surface flux with the bulk medium. This aspect of a tightly bound layer of charges was abandoned by Fixman [54-55] and Chew and Sen [56-57]. Instead, the later two groups incorporated the Gouy-Chapman model of a diffuse double layer in which a potential for the ionic charge cloud was described by a Boltzmann distribution. These latter theories were complicated and, as a consequence, Grosse [58-59] proposed a simplified model. This model preserves the important features of the previous theories, however, offers a few assumptions. The model assumes that the counterion layer is thin and contains only ions which are opposite in sign to that of the fixed charges on the particles, and that the counterions can exchange freely only with ions of the same sign in the bulk electrolyte. More recently, Paul et al [46] proposed a new model to account for the anomalies in the surface conductance of the double layer for very low field frequencies using the tools provided by nonequilibrium statistical mechanics.

In Grosse's model mentioned above, when an electric field is applied, the ions in the system redistribute under the influence of both the field and diffusion. The time constant of the low frequency relaxation in this model was found to be similar to that derived by Schwarz:

$$\tau_{LF} = \frac{r^2}{D} \tag{2.38}$$

but D here is the diffusion coefficient of ions in the bulk electrolyte rather than the surface diffusion constant as described by Schwarz. This relaxation is governed by the radial diffusive motion of ions in the bulk electrolyte and its amplitude is described by:

$$G_{LF} = \frac{9\upsilon\varepsilon_m Z^4 L^4}{16[ZL(L+1)+2]^2} \tag{2.39}$$

where L is the number of counterions per unit area, Z is the quotient of the particles radius and the Debye screening length, and υ is the volume fraction of the particles. The $\underline{K}(\omega)$ expression is shown in Equation 44 in Grosse's paper [59] (described as "dipolar field coefficient"). This expression and other details related to it will not be discussed in this thesis.

CHAPER 3

EXPERIMENT

3.1 Electro-rotation System

A block diagram of the electro-rotation system used in these series of experiments is shown in Fig.3.1. A programmable quardrature sine wave generator produces the signals applied on four spherical electrodes which are monitored by a Tektronix 2213A 60 MHz oscilloscope and the frequency of the field could be controlled by the program [60]. The voltage was fixed at 10 Vpp. The four stainless steel electrodes were successively coated by nickel (10 – 12 μm in thickness), then by gold, and housed in an electrical chamber specially constructed for these experiments. The 5-mm spacing between opposite electrodes (4 mm in diameter) allowed the production of fields up to 700 V/m rms. The dimensions of the chamber were chosen such that the embryo (2 mm in diameter) fitted into the chamber (Fig.3.2). The chamber was mounted on the stage of an optical microscope (Leica MZ6) so that the rotation of the embryo, which was centered between the four electrodes (Fig.3.3), could be observed. The embryo image was magnified and focused into a HITACHI KP-161 video camera aided by the optical microscope. Images of the rotating embryos were both displayed on a TV monitor (Sony) and recorded on videotape using a Panasonic AG-1960 VCR. The rate of rotation of the embryos at different field frequencies were extracted manually from the videotape and plotted.

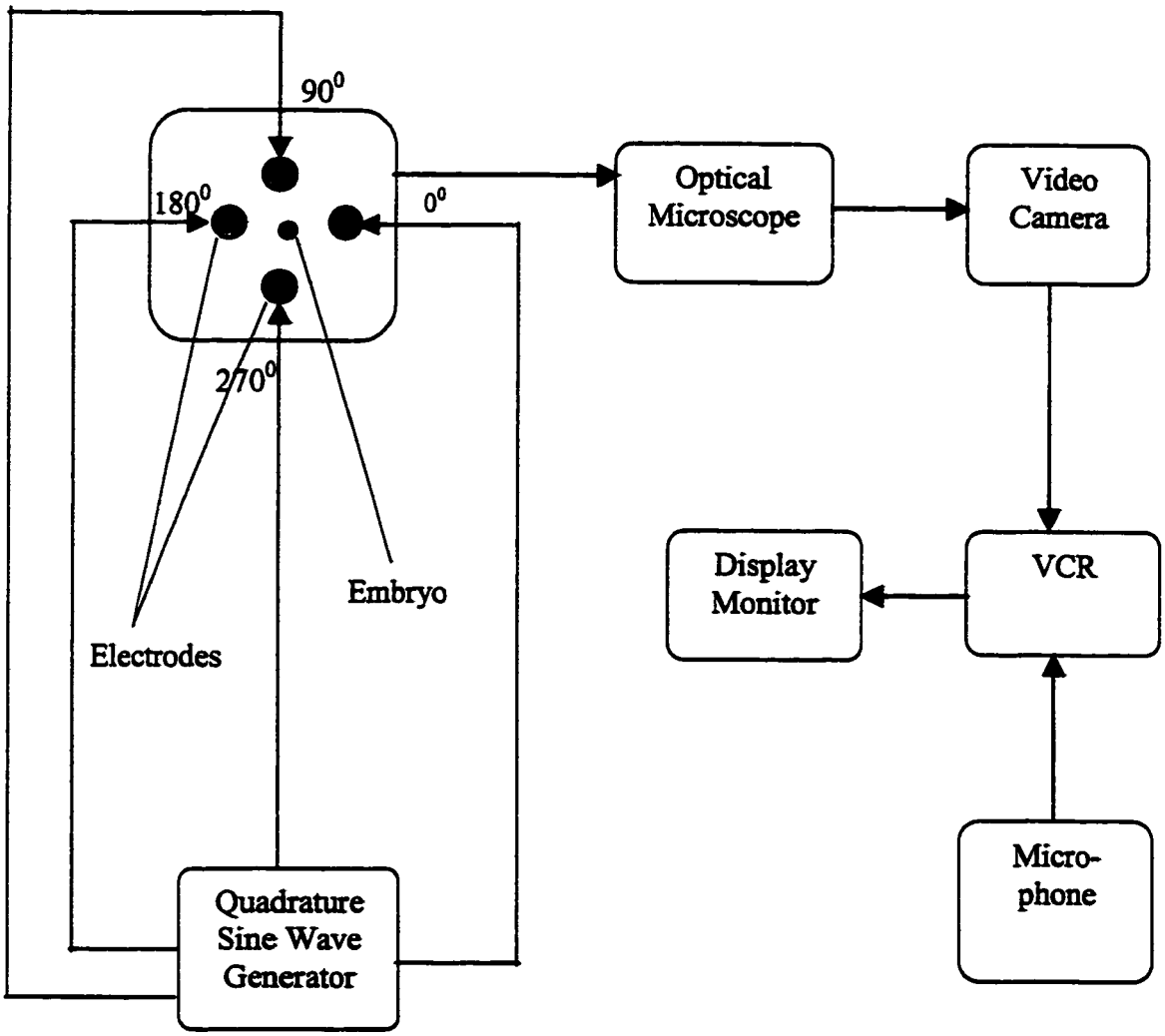

Fig. 3.1 Block diagram for electro-rotation system

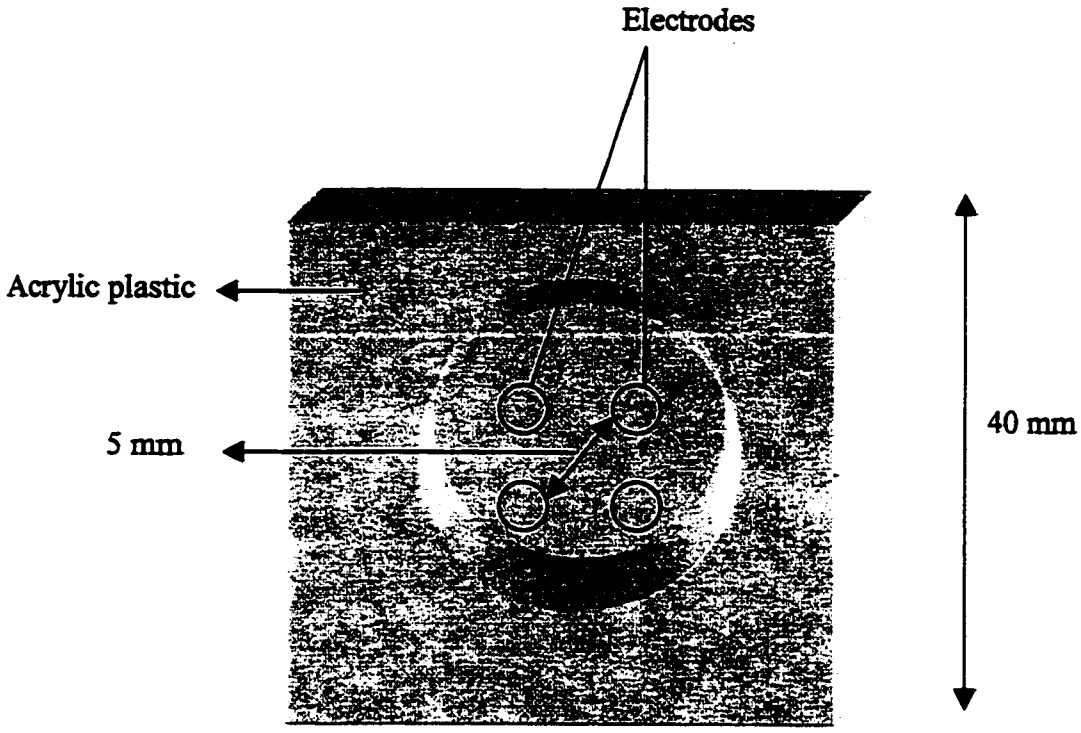

Fig. 3.2 Three-dimensional diagram of electro-rotation chamber

Fig. 3.3 An Axolotl embryo centered between four electrodes

3.2 Preparation of Sample

In these series the following two types of eggs were studied:

(1) Axolotl Eggs:

Several batches of Axolotl eggs, comprised of both embryos and unfertilized eggs, were obtained from the Axolotl colony maintained by Gordon's laboratory in Winnipeg, Manitoba, Canada. The eggs were supplied over a period of one year from occasional natural spawning. They were shipped in cooled thermos (flasks) in order to maintain a low temperature and thus inhibit rapid development. However, a temperature variation amongst the different batches within a range of $12^0C - 16^0C$ was observed, but the specimens were kept in water at temperatures of about $8^0C - 10^0C$ before experimentation. All experiments, however, were carried out at room temperature.

Prior to electro-rotation measurements the three-layered protective jelly coat encasing the embryo was removed mechanically using a pair of fine tweezers. However, the vitelline membrane, tightly surrounding the embryos was left intact since we intended to perform experiments on eggs at early stages, which could be easily damaged in the absence of the vitelline membrane. After dejellying, the eggs were washed three times with the media to be experimented in and centered between the four electrodes in the fore- mentioned medium.

After the preliminary treatment discussed above, electro-rotation measurements were carried out in distilled water and other media of varying conductivities. These conductivities were adjusted by adding NaCl and measured by a conductivity meter (model No. 1710, Bio-Rad Laboratories, Richmond, CA). 25% Holtfreter's medium consisting of 15.00 mM NaCl, 0.17 mM KCl, 0.23 mM $CaCl_2$, and 0.60 mM $NaHCO_3$

(pH 7.4) was also prepared and used for some of the measurements. In addition, a modified Steinberg's solution consisting of 60.00 mM NaCl, 0.67 mM KCl, 0.34 mM Ca $(NO_3)_2$, 0.83 mM $MgSO_4$ and 10.00 mM Tris (pH 7.4) was prepared for experiment and maintaining some embryos. Both, Holtfreter's and Steinberg's solutions have been routinely used by other investigators [61] to maintain dejelled embryos and have shown no effect on embryo's viability.

(2) Xenopus Eggs:

The Xenopus eggs were obtained from the laboratory of Dr. McFarlane, in the Department of Cell Biology and Anatomy at the University of Calgary. These eggs which had been produced by hormone-induced spawning were collected at early stages (1 – 13). The embryos (about 1 mm in diameter) were kept at room temperature prior to and during the experiments. The embryos were stripped out of their jelly coat by a 10-minute immersion in 2% cysteine (pH 7.8 – 8.0) and the embryos were ready for experiment after washing them three times with the suitable medium. All solutions mentioned earlier were used in this round of experiments.

CHAPTER 4

RESULTS AND DISCUSSION

4.1 General Effects of an AC Rotating Electric Field on Axolotl Embryos

The effect of a rotating AC field on Axolotl embryos is summarized in Fig.4.1. The field had no effect on 20% of the 160 gastrulae examined; these embryos seemed to be in good physical condition after 20 – 30 minute exposures to the field and developed normally to later stages. In addition, 7% of the embryos examined showed severe damage (burst completely) in less than a minute after being subjected to a rotating electric field (See Fig.4.2). The remaining 73% of embryos showed irreversible morphological changes and no behavioral abnormalities were studied since the embryos failed to survive such changes (died within a few hours). Morphological changes appeared, as movement of embryonic material from the interior of the embryo to the surface while the vitelline membrane was still intact. In some cases, we observed the breakdown of the vitelline membrane at some point where embryonic material leaked out of the embryo to the medium (Fig.4.3). A closer investigation showed spreading of the larger yolk cells in the vegetal pole to the surface of the embryo while the pigmented cells of the animal pole seemed to invaginate inside the embryo (contraction of the animal cap). The explosive nature of the embryonic discharge suggests excessive pressure build-up in the blastocoel and archenteron cavities of the embryo, which causes the breakdown of the embryo. The question remains how/why pressure builds up as the embryo is exposed to the field, and what mechanisms are involved. The precise nature of the electrically induced damage was not investigated in any detail in this work.

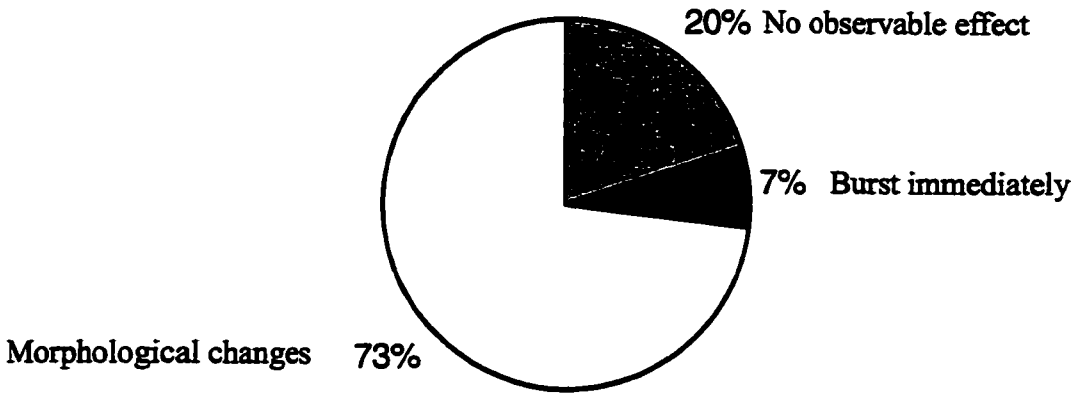

Fig.4.1 Response of Axolotl embryos (gastrulation) to an ac electric field

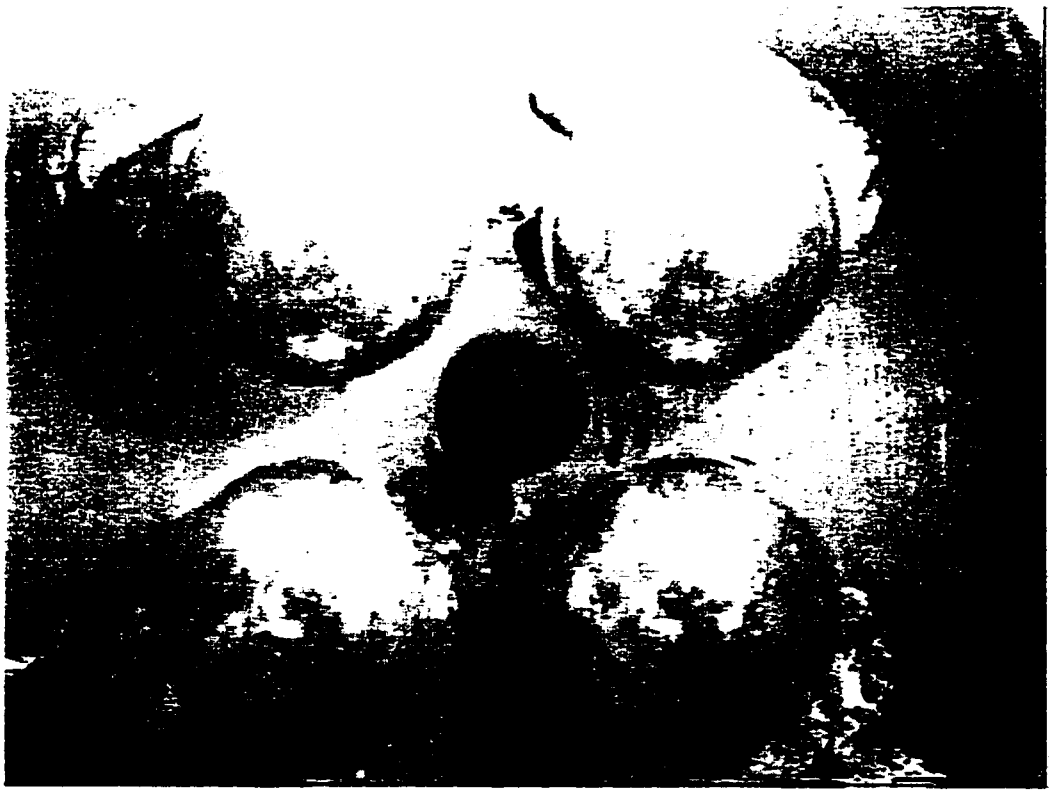

Fig.4.2 Blow-out of an Axolotl embryo after a brief exposure to electric field

Fig. 4.3 Embryonic material leaking out the embryo

4.2 Electro-rotation of Axolotl Embryos: Stages 5 – 9

Initially electro-rotation measurements were carried out on both unfertilized and fertilized eggs (embryos) so that changes in electrical properties after fertilization may be studied/explained. However, no measurable electro-rotation was observed in either the unfertilized eggs or in viable embryos at stages prior to gastrulation (5-9) over the frequency range 100 Hz to 2 MHz. The lack of any electro-rotation over this wide frequency range suggests the absence of any sizable dispersion in the frequency dependent polarization response. Furthermore, this suggests that the vitelline membrane

is quite permeable to ionic transport, and electrically, the outside medium closely resembles the embryo interior. Moreover, it is suggested [62] that during the early stages of embryo development there is a continuous inflow of water at the animal pole region of the embryo and outflow at the vegetal pole. This flow of water gives the interior of the embryo and the medium similar electrical properties (both conductivity and permittivity). This is explained in Equation 2.4 where the Clausius-Mossotti factor vanishes when the complex permittivities of the medium and the embryo are equal and therefore, no rotation is expected.

4.3 Electro-rotation of Axolotl Embryos: Stages 10 –12 (gastrulation)

Rotation of the whole embryo or its interior was evident in about 20% of the 160 gastrulae examined. Electro-rotation spectra, where the embryo rotational velocity is measured as a function of the rotating field frequency, were obtained over the frequency range of 1 kHz to 2 MHz. A typical electro-rotation spectrum, obtained by using electro-rotation measurements, and a simple shelled spherical model spectrum are shown in Figs.4.4 and 4.5 respectively. The embryos, when placed in low conductivity medium (11 μS/cm) exhibited co-field rotation over the frequency range of 700 kHz to 2 MHz, while counter-field rotation was observed in the range of 1 kHz to 50 kHz. These results are consistent with the observations obtained for other biological particles by other researchers [19, 26, 33, 36, 31]. Comparing the experimental results with the model prediction, we can see that the simple shelled spherical model can well represent the electro-rotation behavior in the frequency range mentioned earlier. Typical normalized rotation spectra obtained for Axolotl embryos are shown in Fig.4.6. In order to avoid the

effect of joule heating at low frequencies, electro-rotation measurements were initiated at the high end of the frequency range (this explains the limited amount of counter-field rotation shown in this work), and no investigations below frequency of 100 Hz were carried out. The observed faster rotation at 500 – 700 Hz, which may be related to double layer polarization, was difficult to measure because of joule heating effects. Joule heating caused electrode reactions and rapid damage of embryos. In addition, all embryos failed to rotate when placed in other media prepared (mentioned in section 3.2).

Using the one-shelled theoretical model, where the ectoderm is considered to be the shell in the Axolotl embryo, the capacitance of the ectoderm can be estimated by the following relation [63]:

$$\tau_\alpha \equiv C_{sh}.R/2\sigma_m \qquad (\text{assuming } C_{sh}.R \gg \varepsilon_m) \tag{4.1}$$

Where τ_α = relaxation time (inverse of peak frequency) of counter-field peak.

R = embryo radius.

σ_m = medium conductivity.

ε_m = medium permittivity.

C_{sh} = effective shell capacitance.

From the relaxation time of the low frequency rotation (attributable to Maxwell-Wagner relaxation arising from differential charging of the ectoderm) in Fig.4.1, the capacitance of the ectoderm was calculated to be $4.57^* 10^{-2}$ μF/cm^2. This value is about two orders of magnitude smaller than the one for protoplast membrane or for typical spherical cell bilayer membrane (~1 μF/cm^2). This is reasonable since the ectoderm is not a simple

bilayer membrane structure but by stage 10 consists of a monolayer of cells covering the surface. Warner [64] estimated the diameter of the Axolotl ectodermal cells to be in the range 25-30 μm. However, the thickness of the ectoderm is estimated as 100 μm since the cells are elongated. From both the capacitance and the thickness of the ectoderm, the absolute permittivity of the ectoderm was determined to be 4.5×10^{-8} $C^2/N.m^2$, which yields a relative permittivity value of 5.082×10^3. This relative permittivity value is reasonable as compared to Schwan's [65] summary of various relaxation mechanisms in muscle, tissue structure (Maxwell-Wagner) in particular.

The higher frequency relaxation (700kHz to 2 MHz) in Fig.4.1 allows us to determine the permittivity of the embryo, ε_{in}, using the following relation for the relaxation time [63]:

$$\tau_\beta \cong (\varepsilon_{in} + 2\varepsilon_m)/\sigma_{in} \qquad \text{(assuming } \sigma_{in} \gg \sigma_m\text{)} \qquad (4.2)$$

The conductivity of the embryo, σ_{in}, was measured (~ $0.2501*10^2$ S/m) while the calculated values of the permittivities of embryos at different stages are summarized in Table 4.1. Such high dielectric constants (permittivities) shown in Table 4.1 are similar to the values obtained for live tissues by Schwan although two different techniques were used [65].

4.4 Electro-rotation of Axolotl Embryos: Stages 14 – 16 (neurulation)

A similar experimental procedure was used to examine the electro-rotation behavior of embryos at stages 14 to 16 (beginning of neurulation stages). However, no rotation was observed at these stages in about 30 embryos examined in various media.

A possible explanation for the lack of rotation in the 80% of gastrulae and all neurulae investigated is the presence of a permanent polarization. We suggest that the Axolotl embryo has a permanent dipole moment that opposes the induced dipole moment produced by the applied field, so that a small resultant rotation ensues. The fact that Axolotl embryos are considered to be electrically polarized [66] encourages us to suggest/consider a permanent dipole moment. To explain, a polarized ionic current was found to leak out of the blastopore throughout the gastrula and neurula stages of the Axolotl [20]. To an external field the source (point of higher potential) and sink (point of lower potential) of the charges constituting the current, would appear as a permanent dipole which could make a significant contribution to the overall polarizability and hence rotation rate of the embryo. The exact pathway of these currents inside the embryo is not really known. However, it is suggested that blastopore currents might be controlled by junctional changes in the archenteron wall.

In this work, the electro-rotation theory is extended to include the permanent dipole contribution. Details of the analysis required to incorporate the effects of this permanent dipole moment are presented in the next chapter. As the model will show later, rotational torques due to the two different dipoles, induced by the applied external field and permanent, are predicted to be opposite in direction, and therefore, no rotation is expected when they are equal in magnitude.

4.5 Electro-rotation of Xenopus Embryos: Stages 1 – 16

No rotation was observed in Xenopus embryos at all stages examined (1 – 16). We have no clear suggestions/reasons for this lack of rotation. However, this piece of

information shows a possible correlation with other observations in literature. To explain, Nieuwkoop et al [67] reported surface contraction and expansion waves in Axolotl embryos, however no such waves were observed in Xenopus embryos. These waves, which travel at rate of few micrometers per second, were found to traverse the surface (3mm deep) of Axolotl embryos during the gastrulation stages. Thus, it seems that the rotation phenomenon in Axolotl might be correlated with these waves. This suggestion is preliminary and further investigation has to be done to verify or refute this idea.

Table 4.1: Relative permittivity values of Axolotl embryos at various stages of development

Stage of Embryo	**Relative permittivity**
10	$1.5 * 10^6$
10.5	$1.7 * 10^6$
11	$1.4 * 10^6$
12	$1.6 * 10^6$

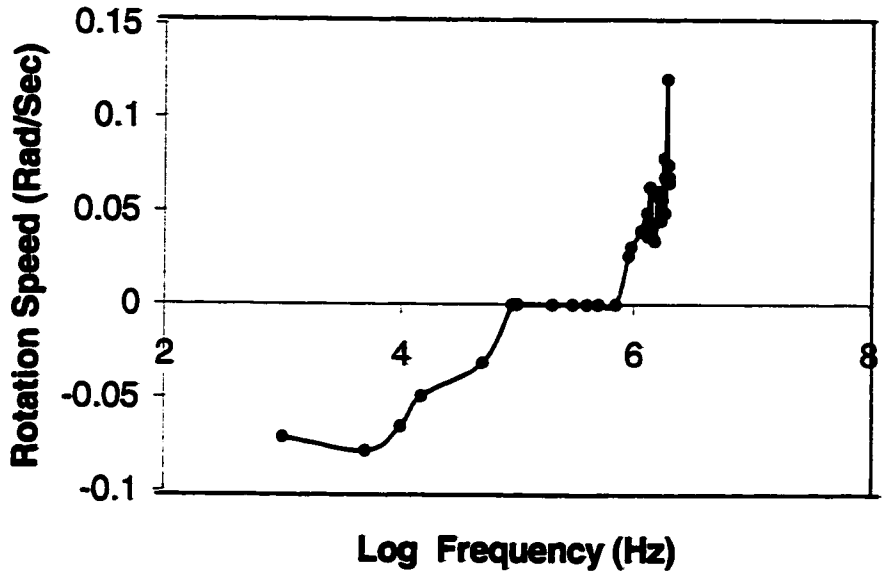

Fig.4.4 Electro-rotation spectrum of an Axolotl embryo: Stage 11, medium conductivity = 11μS/cm

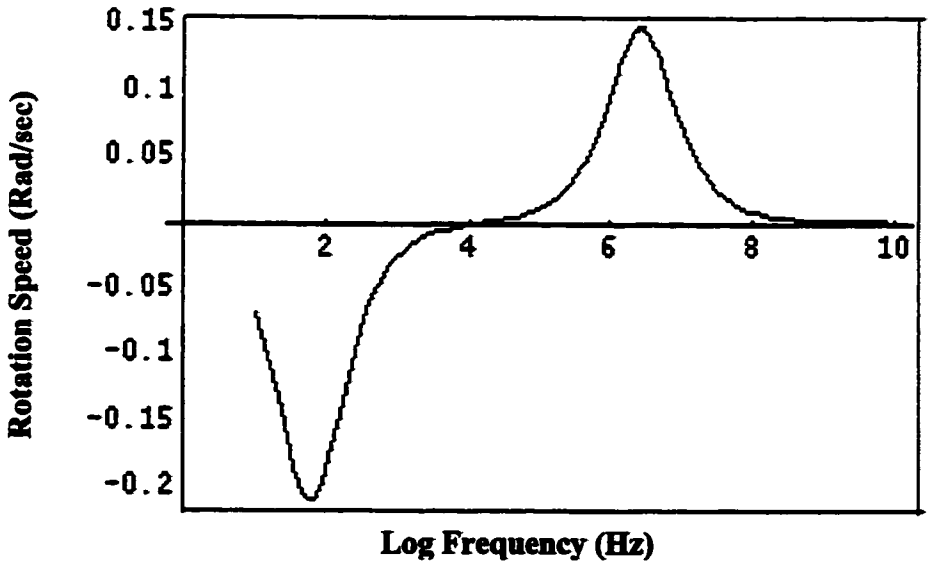

Fig. 4.5 Electro-rotation theoretical spectrum: Rotation speed as a function of field frequency ($\varepsilon_m = 78\varepsilon_0$, $\varepsilon_{in} = 60\varepsilon_0$, $R = 1$mm, $C_{sh} = 0.5\mu F/cm^2$, $\sigma_m = 10\mu S/cm$, $\sigma_{in} = 2.501*10^5 \mu S/cm$)

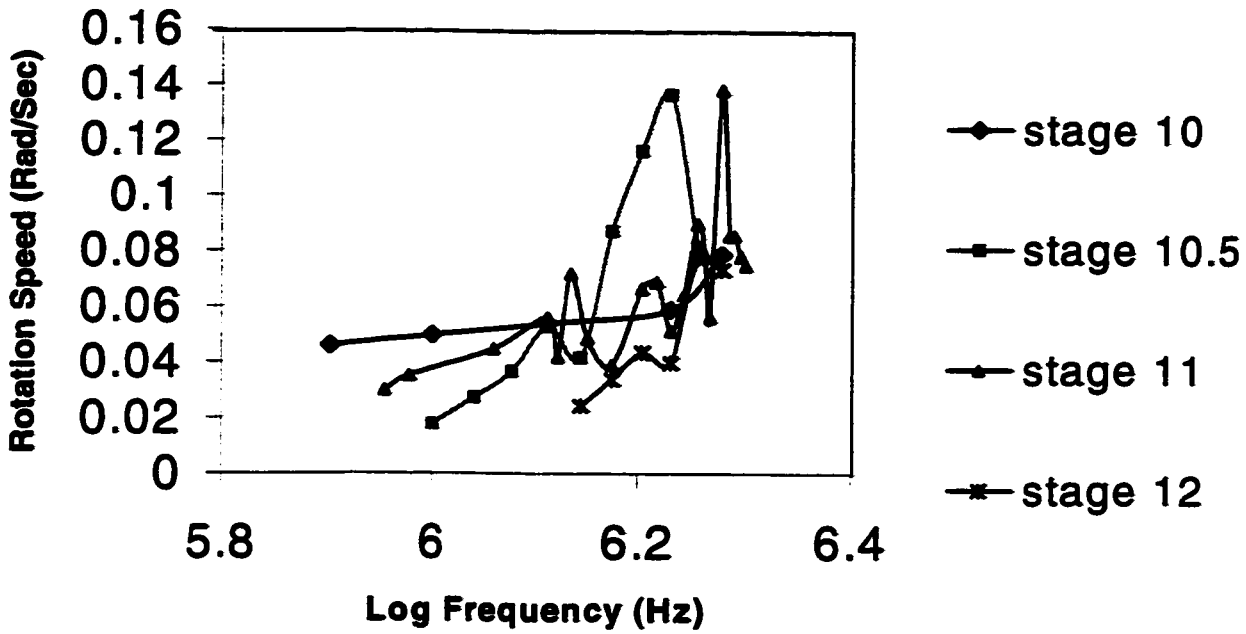

Fig. 4.6 Radius-normalized electro-rotation spectra: Medium conductivity = 11 μS/cm.

CHAPTER 5

THEORETICAL MODEL- INCLUSION OF A PERMANENT DIPOLE MOMENT

Consider a shelled spherical particle of inside permittivity ε_1 immersed in a medium of permittivity ε_3, as shown in Fig.5.1. The inner sphere has a radius 'a' while the outer sphere has a radius 'b' and ε_2 is the permittivity of the shell.

To model the permanent polarization, two point charges $+q$ and $-q$, located at the vector $+\bar{l}$ and $-\bar{l}$ from the origin of the particle, are introduced. The first components in each of the vectors $+\bar{l}(l,\alpha,\beta)$, $-\bar{l}(l,\pi-\alpha,\beta+\pi)$ and $\bar{r}(r,\theta,\phi)$ shown in Fig.5.1 represents the length of the vector. The second and the third components are the polar angle from the z-axis and the azimuthal angle respectively.

We begin the analysis by retaining all the electrical moments (monopoles, dipoles, quadrupoles, etc.) and then consider the specific case of dipole moments only. The response to two sets of charges must be considered in this model:

(1) Charges placed on the electrodes producing the external field. At an arbitrary point P, characterized by the spherical coordinates (r, θ, ϕ) the corresponding potential is given by:

$$\Psi_{ext}(r,\theta,\phi)=\sum_{n=0}^{\infty}\sum_{m=-n}^{n}E_{nm}r^{n}Y_{nm}(\theta,\phi) \qquad \text{(See Appendix B)} \qquad (5.1)$$

Where E_{nm} are the expansion coefficients, determined uniquely by the applied field.

(2) Charges $+q$ and $-q$ constituting the permanent dipole within the particle. In order to calculate the potential, $\bar{r}$ can be considered a variable vector that can lie in any of the

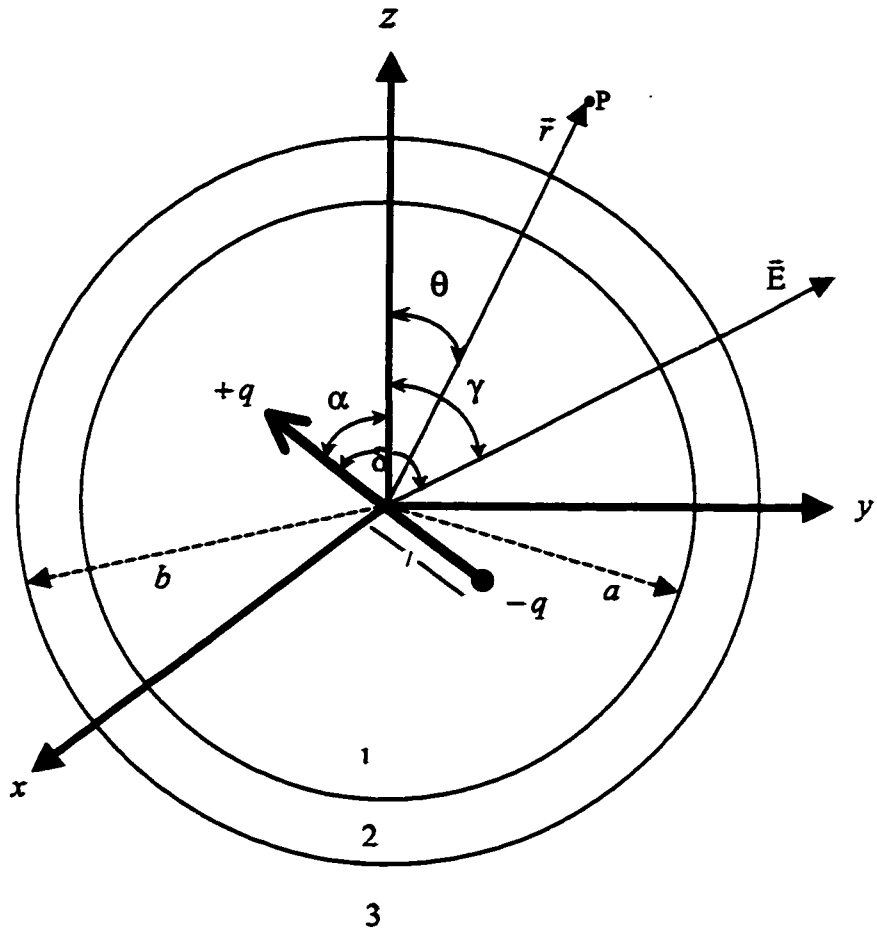

Fig.5.1 A simple shelled spherical model for biological particles with a permanent dipole.

regions 1, 2, or 3 in Fig.5.1. The potential in region1 (the inside) due to charges $+q$ and $-q$ are ψ_+ and ψ_- respectively:

$$\psi_+ = \frac{q}{4\pi\varepsilon_1 |\vec{r} - \vec{l}|} \tag{5.2}$$

$$\psi_- = \frac{-q}{4\pi\varepsilon_1 |\vec{r} + \vec{l}|} \tag{5.3}$$

Jackson has shown that if $|\vec{r}| > |\vec{l}|$, then Equations (5.2) and (5.3) can be written in terms of spherical harmonics [68]:

$$\psi_+ = \frac{q}{\varepsilon_1} \sum_{n=0}^{\infty} \sum_{m=-n}^{n} \frac{1}{2n+1} \frac{l^n}{r^{n+1}} Y^*_{nm}(\alpha, \beta) Y_{nm}(\theta, \phi) \tag{5.4}$$

$$\psi_- = \frac{-q}{\varepsilon_1} \sum_{n=0}^{\infty} \sum_{m=-n}^{n} \frac{1}{2n+1} \frac{l^n}{r^{n+1}} Y^*_{nm}(\pi - \alpha, \pi + \beta) Y_{nm}(\theta, \phi) \tag{5.5}$$

Thus the total potential due to the charges in the inner sphere will be given by:

$$\Psi_{charge}(r, \theta, \phi) = \frac{q}{\varepsilon_1} \sum_{n=0}^{\infty} \sum_{m=-n}^{n} \frac{1}{2n+1} \frac{l^n}{r^{n+1}} \left[Y^*_{nm}(\alpha, \beta) - Y^*_{nm}(\pi - \alpha, \pi + \beta) \right] Y_{nm}(\theta, \phi) \tag{5.6}$$

A term that arises from the external charges should be added to the potential given

in Equation (5.6). Thus, the final potential distribution though the various regions will be as follows:

$$\Psi_1(r,\theta,\phi)=\frac{q}{\varepsilon_1}\sum_{n=0}^{\infty}\sum_{m=-n}^{n}\frac{1}{2n+1}\frac{l^n}{r^{n+1}}\left[Y_{nm}^*(\alpha,\beta)-Y_{nm}^*(\pi-\alpha,\pi+\beta)\right]Y_{nm}(\theta,\phi) \qquad 0<r\le a \quad (5.7)$$
$$+\sum_{n=0}^{\infty}\sum_{m=-n}^{n}A_{nm}r^nY_{nm}(\theta,\phi)$$

$$\Psi_2(r,\theta,\phi)=\sum_{n=0}^{\infty}\sum_{m=-n}^{n}B_{nm}r^nY_{nm}(\theta,\phi)+\sum_{n=0}^{\infty}\sum_{m=-n}^{n}C_{nm}r^{-(n+1)}Y_{nm}(\theta,\phi) \qquad a\le r\le b \quad (5.8)$$

$$\Psi_3(r,\theta,\phi)=\sum_{n=0}^{\infty}\sum_{m=-n}^{n}N_{nm}r^{-(n+1)}Y_{nm}(\theta,\phi)-\sum_{n=0}^{\infty}\sum_{m=-n}^{n}E_{nm}r^nY_{nm}(\theta,\phi) \qquad r\ge b \quad (5.9)$$

In this model, there are no isolated charges, or monopoles and the dominant contribution is dipolar so all the summations are taken at $n=1$. Therefore we rewrite Equations (5.7), (5.8), and (5.9), setting $n=1$ and solve for the constants A_{1m}, B_{1m}, C_{1m}, and N_{1m} using the following boundary conditions:

$$\Psi_1(a,\theta,\phi)=\Psi_2(a,\theta,\phi) \quad (5.10)$$

$$\Psi_2(b,\theta,\phi)=\Psi_3(b,\theta,\phi) \quad (5.11)$$

$$\varepsilon_1(\partial_r\Psi_1)_{r=a}=\varepsilon_2(\partial_r\Psi_2)_{r=a} \quad (5.12)$$

$$\varepsilon_2(\partial_r\Psi_2)_{r=b}=\varepsilon_3(\partial_r\Psi_3)_{r=b} \quad (5.13)$$

The solution for N_{1m} is as follows:

$$N_{lm} = \lambda_1 M_{lm} + \lambda_2 E_{lm} \qquad r \geq b \quad (5.14)$$

Where,

$$M_{lm} = \frac{ql}{3}\left\{Y^*_{lm}(\alpha,\beta) - Y^*_{lm}(\pi-\alpha,\pi+\beta)\right\} \quad (5.15)$$

$$\lambda_1 = \frac{9\varepsilon_2 b^3}{\Delta}; \quad (5.16)$$

$$\lambda_2 = \frac{b^6(\varepsilon_1+2\varepsilon_2)(\varepsilon_2-\varepsilon_3)+a^3b^3(\varepsilon_1-\varepsilon_2)(2\varepsilon_2+\varepsilon_3)}{\Delta} \quad (5.17)$$

$$\Delta = 2a^3(\varepsilon_1-\varepsilon_2)(\varepsilon_2-\varepsilon_3)+b^3(\varepsilon_1+2\varepsilon_2)(\varepsilon_2+2\varepsilon_3) \quad (5.18)$$

The first term in N_{lm} arises from the two charges $+q$ and $-q$ (permanent dipole moment) inside the particle while the second term represents the dipole moment induced by the external charges (external applied field) and leads to the conventional Clausius-Mossotti factor, λ_2, of a shelled particle. It is imperative to keep in mind the fact that the permanent dipole owing to its presence in a polarizable environment results in an induced dipole in the latter. And it is this aspect of the problem that manifests itself through the parameter λ_1, which therefore, plays a similar role to the Clausius-Mossotti factor λ_2. The combination of the permanent dipole and the associated induced dipole (results as a consequence of the presence of the permanent dipole in a polarized medium) will be referred to as the *net permanent dipole*. In electro-rotation experiments where the torque is determined by the angle between a dipole and the external field, the differing phase lags of the various dipoles become significant.

To make progress towards calculating the potential outside the particle, we assume that the external field can be described by $\vec{E}(E_0,\gamma,\varphi)$ where E_0 is the magnitude, γ is the polar angle with respect to the z-axis and φ is the azimuthal angle. Analogous to the definition of the dipole moment in Equation (5.15), the electric field is defined by employing spherical harmonics shown in appendix B. Substituting equations B.4-B.12 into Equations (5.14) and (5.9), the potential at point P is obtained:

$$\Psi_{outside}(r,\theta,\phi)=\frac{\lambda_1 ql}{2\pi r^2}(Sin\alpha.Cos\beta.Sin\theta.Cos\phi+Sin\alpha.Sin\beta.Sin\theta.Sin\phi+Cos\alpha.Cos\theta)$$
$$+\frac{\lambda_2 E_0}{r^2}(Sin\gamma.Cos\varphi.Sin\theta.Cos\phi+Sin\gamma.Sin\varphi.Sin\theta.Sin\phi+Cos\gamma.Cos\theta) \quad (5.19)$$

Now, consider three unit vectors:

$$\vec{e}_M=\begin{pmatrix}Sin\alpha\ Cos\beta\\ Sin\alpha\ Sin\beta\\ Cos\alpha\end{pmatrix};\quad \vec{e}_E=\begin{pmatrix}Sin\gamma\ Cos\varphi\\ Sin\gamma\ Sin\varphi\\ Cos\gamma\end{pmatrix};\quad \vec{e}_r=\begin{pmatrix}Sin\theta\ Cos\phi\\ Sin\theta\ Sin\phi\\ Cos\theta\end{pmatrix} \quad (5.20)$$

Then Equation (5.19) can be written in a compact simplified form:

$$\Psi_{outside}(r,\theta,\phi)=(\lambda_1 M\varepsilon_3\vec{e}_M+4\pi\varepsilon_3\lambda_2 E_0\vec{e}_E).\frac{1}{4\pi\varepsilon_3 r^2}\vec{e}_r \quad (5.21)$$

Where $M=2ql$ is the permanent dipole moment. Equation (5.21) can be written short-handed as follows:

$$\Psi_{outside}(r,\theta,\phi)=\frac{\vec{P}.\vec{e}_r}{4\pi\varepsilon_3 r^2} \quad (5.22)$$

Where $\vec{P}$ is the total dipole moment. Experimentally, the problem is restricted to the xy-plane thus eliminating dependence on the azimuthal angles β and ϕ then the net permanent and the field-induced dipole moments are given as follows:

$$\vec{P}_{per} = \lambda_1 M \varepsilon_3 (\vec{i} Cos\alpha + \vec{j} Sin\alpha) \tag{5.23}$$

$$\vec{P}_{ind} = 4\pi\varepsilon_3 E_0 \lambda_2 (\vec{i} Cos\gamma + \vec{j} Sin\gamma) \tag{5.24}$$

In a typical electro-rotation experiment, the applied field is time-dependent and rotating in xy-plane:

$$\gamma = \omega\tau \tag{5.25}$$

Defining the field in the following phasor notation:

$$\underline{\vec{E}}(\tau) = Re\left[E_0 (\vec{i} - i\vec{j}) e^{i\omega\tau}\right] \tag{5.26}$$

And, in order to account for the phase lags of both the net permanent and field induced dipole moments the parameters λ_1 and λ_2 are made complex. The total dipole moment (the net permanent dipole and the field-induced dipole) can then be written as follows:

$$\underline{\vec{P}} = \underline{\lambda}_1 M \varepsilon_3 (\vec{i} - i\vec{j}) e^{i\alpha(\tau)} + 4\pi\varepsilon_3 E_0 \underline{\lambda}_2 (\vec{i} - i\vec{j}) e^{i\omega\tau} \tag{5.27}$$

The torque may be calculated from Equations (5.26) and (5.27) using the standard formula:

$$\underline{\vec{T}} = \underline{\vec{P}} \times \underline{\vec{E}} \tag{5.28}$$

Which leads to the following:

$$\vec{T} = \vec{k}\left[M\varepsilon_3 E_0 (Re[\underline{\lambda}_1] Sin(\omega\tau - \alpha) - Im[\underline{\lambda}_1] Cos(\omega\tau - \alpha)) - 4\pi\varepsilon_3 E_0^2 \, Im[\underline{\lambda}_2]\right] \tag{5.29}$$

Where $\delta = \alpha - \omega\tau$ is the angle between the electric field and the permanent dipole moment vector. Taking $\delta = \pi/2$ and considering the real parameters only, the result in Equation (5.29) is found to be consistent with Jones [63] work on a particle with permanent magnetic moment subjected to a magnetic rotating field. In such case, a co-field rotation is predicted (maximum torque) and the lag angle is derived:

$$\delta = Sin^{-1}\left[\frac{8\pi\eta R^3\omega}{ME_0}\right] \tag{5.30}$$

Since a time-dependent field is present and the system (medium and particle) is lossy, the particle can't keep up with the field and, therefore, the net permanent dipole lags behind the rotating external field by χ:

$$\chi = Tan^{-1}\left[\frac{Im[\underline{\lambda}_1]}{Re[\underline{\lambda}_1]}\right] \tag{5.31}$$

This lag can be accounted for by writing:

$$\underline{\lambda}_1 = |\lambda_1| e^{i\chi} \tag{5.32}$$

$$Re[\underline{\lambda}_1] = |\lambda_1| Cos\chi \tag{5.33}$$

$$Im[\underline{\lambda}_1] = |\lambda_1| Sin\chi \tag{5.34}$$

Substituting Equations (5.33) and (5.34) into (5.29), the total torque becomes:

$$\vec{T} = \{ME_0\varepsilon_3|\lambda_1|Sin(\delta - \chi) - 4\pi\varepsilon_3 E_0^2\, Im[\underline{\lambda}_2]\}\vec{k} \tag{5.35}$$

Here δ as shown as mentioned earlier (see Fig. 5.1) is the angle between the external field and the permanent dipole moment vector. From a practical point of view, at this

stage, information about the angle δ is lacking hence assuming the special case where the permanent and external field lie in the same direction ($\delta = 0$) the total torque can be expressed by:

$$\bar{T} = \{-ME_0\varepsilon_3 \, \mathrm{Im}[\underline{\lambda}_1] - 4\pi\varepsilon_3 E_0^2 \, \mathrm{Im}[\underline{\lambda}_2]\}\bar{k} \qquad (5.36)$$

The first part of equation (5.36) represents the contribution of the permanent dipole moment while the second part of this equation represents the torque arising from the field-induced dipole moment (the conventional model). Using the same set of parameters where applicable, graphical representation (electro-rotation spectra) of both parts, induced and permanent are shown in Figs.5.2 and 5.3 respectively. The total torque (Equation (5.36)) as a function of field frequency is shown in Fig.5.4. From this figure, we can see that the permanent dipole model explains the lack of rotation at high frequencies when the magnitude of the permanent dipole is in the order of 10^{-15} C.m.. The permanent dipole moment has no contribution in the low frequency region, and therefore, this model has difficulties explaining the rotational behavior in this frequency region.

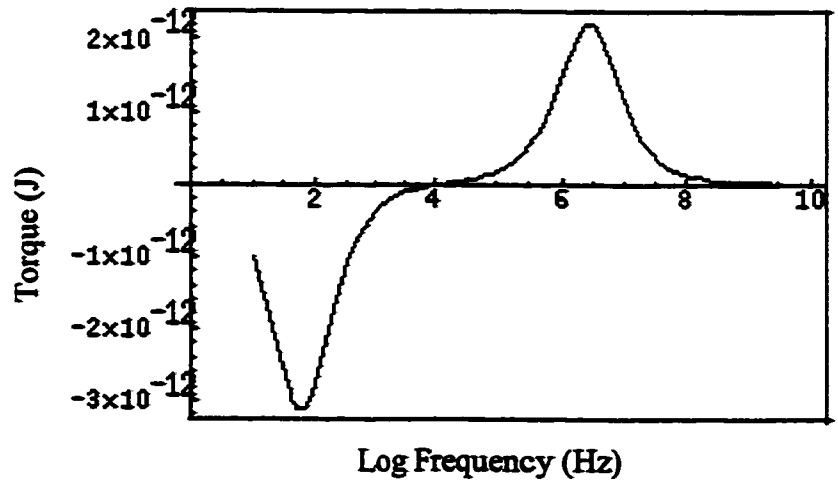

Fig.5.2. Theoretical spectrum: Torque induced by the electric field. $\varepsilon_1 = 60\varepsilon_0$, $\varepsilon_3 = 78\varepsilon_0$, $\sigma_1 = 0.03$ s/m, $\sigma_3 = 10^{-3}$ s/m, $C_{sh} = 1\mu$F/cm^2, $E_0 = 707.11$ V/m, $b = 1$ mm)

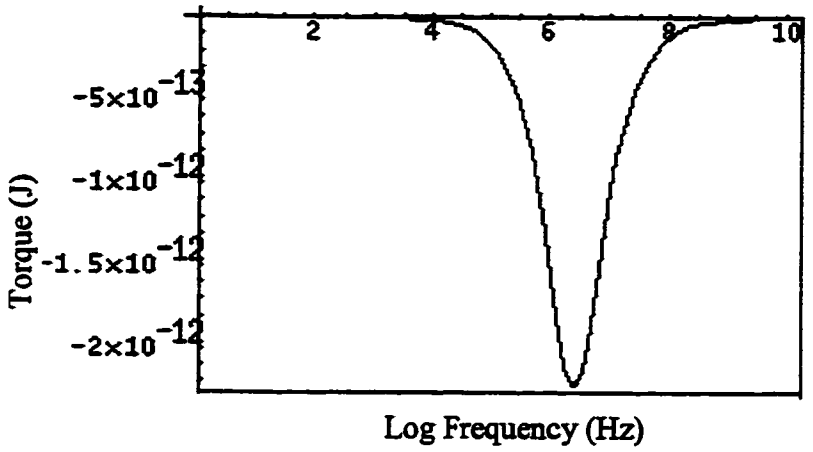

Fig.5.3. Theoretical spectrum: Torque due to permanent dipole moment.

($\varepsilon_1 = 60\varepsilon_0$, $\varepsilon_3 = 78\varepsilon_0$, $\sigma_1 = 0.03$ s/m, $\sigma_3 = 10^{-3}$ s/m, $C_{sh} = 1\mu F/cm^2$, $E_0 =$ 707.11 V/m, $b = 1$mm, $M = 2.67*10^{-15}$ C.m.)

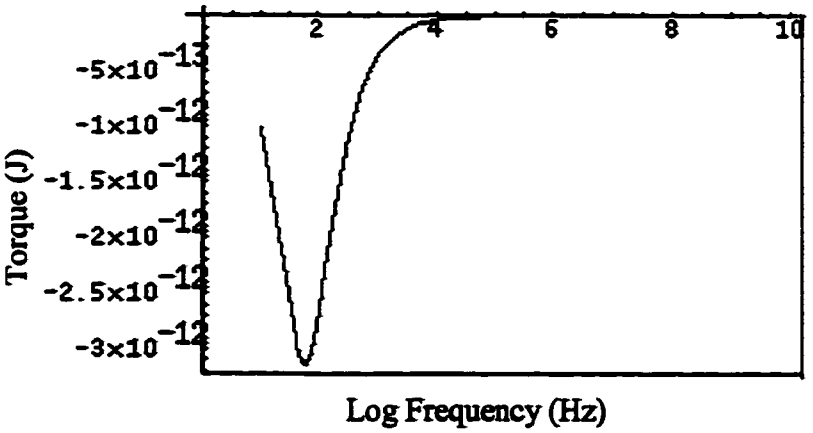

Fig.5.4. Total Torque: Induced and permanent dipoles.

($\varepsilon_1 = 60\varepsilon_0$, $\varepsilon_3 = 78\varepsilon_0$, $\sigma_1 = 0.03$ s/m, $\sigma_3 = 10^{-3}$ s/m, $C_{sh} = 1\mu F/cm^2$, $E_0 = 707.11$ V/m, $b = 1$ mm, $M = 2.67*10^{-15}$ C.m.)

CHAPTER 6

CONCLUSIONS

For the first time, electro-rotation measurements have been conducted on individual Axolotl embryos in low conductivity media. From such measurements, the ectoderm capacitance and the effective permittivity of the embryo were determined utilizing the simple-shelled spherical model. However, the simple-shelled model and other dielectric cell models could not satisfactorily explain all the experimental observations, the lack of rotation at certain stages of development in particular. Therefore, a new theoretical model incorporating a permanent dipole moment was proposed. The permanent dipole was introduced in order to simulate the source of both endogenous currents and associated fields in the intact viable embryos. Such a model did indeed explain the rotational behavior of Axolotl embryos at some particular stages of embryogenesis.

The medium conductivity was the only other parameter varied besides the different sizes of embryos. Embryos immersed in media of conductivity ranging from 40 – 600 μS/cm failed to rotate. However, embryos at gastrulation stages showed both counter- and co-field rotations when immersed in distilled water (11 μS/cm). Moreover, embryos with larger radii exhibited a lower co-field characteristic frequency (frequency corresponding to the peak).

The field strength was kept fixed at ~ 7 Vcm^{-1} throughout all measurements. Varying the field strength so that the dependence of embryo rotation speed on applied external field can be studied is a possible future investigation. As shown in Equation

(5.36), the field-induced rotation is proportional to E^2 while the rotation due to permanent dipole depends only on E magnitude instead. Hence, measuring the speed of rotation at different field magnitudes would be a helpful investigation to further justify the permanent dipole moment. In addition, different electrode geometry (for example needle or planar electrodes) and dimensions should be attempted in order to minimize the joule heating effect at low frequencies. Smaller dimensions (distances between electrodes and chamber thickness) will result in smaller field strength; thus, less joule heating effects would result. With the present measurement system, the rotating embryo image is recorded on the video tape and processed later. To save time, a future improvement could include a real-time cell motion detection. An inconvenient feature of the chamber used was the difficulty of centering the egg between the four electrodes since the embryo's density is close to the density of water. To eliminate this problem, a chamber with a cavity that can hold the embryo at a certain position should be constructed.

Electro-rotation measurements can be extended to later stages of development where the embryos no longer retain their spherical shapes. Measurements of this type would enable the development of more appropriate models suitable to multi-cellular systems. A model, which considers the boundary conditions between single cells in the outer layer, would represent the Axolotl embryos more accurately. It is also useful to extend the measurements to higher ranges of field frequencies in order to facilitate a comprehensive examination of the relaxation spectrum.

Electro-rotation, although proven non-invasive for small biological particles, seems to damage the more fragile Axolotl embryos. An alternate approach would be to use impedance spectroscopic methods at the single embryo level.

REFERENCES

1. Pohl, H.A. and Crane, J.S., "Dielectrophoresis of cells", *Biophys. J.*, **11**, pp.711 (1971).
2. Pohl, H.A., "Dielectrophoresis: Applications to the characterization and separation of cell", in *Methods of cell separation*, Catsimpoolas, N., Plenum Press, New York, pp.67 – 169 (1978).
3. Zimmermann, U. and Scheurich, P., "High frequency fusion of plant protoplasts by electrical fields", *Planta*, **151**, pp. 26 (1981).
4. Pohl, H.A., *Dielectrophoresis: The behavior of matter in nonuniform electric fields*, Cambridge University Press, London (1978).
5. Kell, D.B., "The principles of potential of electrical admittance spectroscopy: an introduction" in *Biosensors: Fundamentals and applications*, Turner, A.P.F., Karube, I. And Wilson, G.S., Oxford University Press, Oxford, 429 – 470 (1986).
6. Pohl, H.A., "Oscillating fields about growing cells", *Int. J. Quantum Chem.*, **7**, pp.411 – 431 (1980).
7. Cambiaso, A. and Grattarola M., "Electrically induced cell manipulation", *Biophys. J.*, **34**, pp.505 – 515 (1987).
8. Schwan, H.P., "Electrical properties of tissue and cell suspensions", *Adv. Biol. Med. Phys.*, **5**, pp.147 – 209 (1957).
9. Hanai, T., Asami, K. and Koizumi, n., "Dielectric theory of concentrated suspensions of shelled-spheres in particular reference to the analysis of biological cell suspensions", *Bull. Inst. Chem. Res. Kyoto Univ.*, **57**, pp.297 - 305 (1979).

10. Takashima, S., Asami, K. and Takahashi, T., "Frequency-domain studies of impendence characteristics of biological cells using micropipette techniques", *Biophys. J.*, **54**, pp.995-1000 (1988).

11. Obi, I., Ichiaki, Y., Nonaka, R. and Senda, M., "Electrophoretic studies on plant protoplasts, relative amounts of various charged groups on the surface of barley mesophyll protoplasts", *Plant Cell Physiol.*, **30 (5)**, pp.759-764 (1989).

12. Kaler, K.V.I.S. and Jones, T.B., "Dielectrophoresis spectra of single cells determined by feedback-controlled levitation", *Biophys. J.*, **57**, pp.93 (1990).

13. Jones, T.B. and Kallio, G.A., "Dielectrophoretic levitation of spheres and shells", *J. Electrostst.*, **6**, pp.207-224 (1979).

14. Arnold, W.M., Schwan, H.P. and Zimmermann, U., "Rotating-field-induced rotation and measurement of the membrane capacitance of single mesophyll cells of avena sativa", *Z. Naturforsch.*, **37c**, pp.908-915 (1982).

15. Fuhr, G., Hagedorn, R. and Goring, H., "Separation of different cell type by rotating electric fields", *Plant and Cell Physiol.*, **26**, pp.1527 (1985).

16. Glaser, R., Fuhr, G. and Gisma, J., "Rotation of erythrocytes, Plant cells and protoplasts in an outside rotating electric field", *Studia Biophys.*, **96**, pp.11-20 (1983).

17. Arnold, W.M., Schmutzler, R.K., Al-Hasani, S. Krebs, D. and Zimmermann, U., "Differences in membrane properties between unfertilised and fertilised single rabbit oocytes demonstrated by electro-rotation. Comparison with cells from early embryos", *Biochimica et Biophysica Acta.*, **979**, pp.142-146 (1989).

18. Sauer, F.A. and Schlögl, R.W., "Torques exerted on cylinders and spheres by external electromagnetic fields: a contribution to the theory of field induced cell rotation" in

Interactions between electromagnetic fields and cells, Chiabrera, A., Nicolini, C. and Schwan, H.P., Plenum Press, New York, pp.203-251 (1985).

19. Müller, T., Fuhr, G., Geissler, F. and Hagedorn, R., "Rotation spectra of mouse eggs up to 35 MHz: Experiments and theoretical interpretation", *Studia Biophysica*, **139 (2)**, pp.77-94 (1990).
20. Metcalf, M.E.M., Shi, R. and Borgens, R.B., "Endogenous ionic currents and voltages in amphibian embryos", *J. Expt. Zool.*, **268**, pp.307-322 (1994).
21. Quincke, G., "Ueber Rotationen im constanten electrischen Felde", *Ann. Phys. Chem.*, **59**, pp.417 (1896), cited in *Electromanipulation of cells*, Zimmermann, U. and Neil, G.A., CRC Press, New York (1996).
22. Lampa, A., "Uber rotationen im elektrostatischen drehfelde", *Wien. Ber.*, **115 (2a)**, pp.1659-1690 (1906), cited in *Electromanipulation of cells*, Zimmermann, U. and Neil, G.A., CRC Press, New York (1996).
23. Teixeira-Pinto, A.A., Nejelski, L.L., Cutler, J.L. and Heller, J.H., "The behaviour of unicellular organisms in an electromagnetic field", *Exp. Cell Res.*, **20**, pp.548 (1960), cited in *Electromanipulation of cells*, Zimmermann, U. and Neil, G.A., CRC Press, New York (1996).
24. Zimmermann, U., Vienken, J. and Pilwat, G., "Rotation of cells in an alternating electric field: The occurrence of a resonance frequency", *Z. Naturforsch.*, **36 (c)**, pp.173 (1981).

25. Arnold, B.M., Geier, B. Wendt and Zimmermann, U., "The change of electro-rotation of yeast cells affected by silver ions", *Biochimica et Biophysica Acta,* **889**, pp.35-48 (1986).

26. Arnold, W.M., Schmutzler, R.K., Schmutzler, A.G., Ven, H. van der, Al-Hasani, S., Krebs, D. and Zimmermann, U., "Electro-rotation of mouse oocytes: Single-cell measurements of zona-intact and zona-free cells and of the isolated zona pellucida", *Biochimica et Biophysica Acta,* **905**, pp.454-464 (1987).

27. Arnold, W.M., Schwan, H.P. and Zimmermann, U., "Surface conductance and other properties of latex particles measured by electrorotation", *J. Phys. Chem.,* **91**, pp.5093-5098 (1987).

28. Arnold, W.M. and Zimmermann, U., "Measurement of dielectric properties of single cells or other particles using direct observation of electrorotation", *The first international conference on low-cost experiment in biophysics,* Cairo University, December 18-20 (1989).

29. Fuhr, G. and Kuzmin, P.I., "Behaviour of cells in rotating electric fields with account to surface charges and cell structures", *Biophys. J.*, **50**, pp.789-795 (1986).

30. Fuhr, G., Glaser, R. and Hagedorn, R., "Rotation of dielectrics in a rotating electric high-frequency field: Model experiments and theoretical explanation of rotation effect of living cells", *Biophys. J.*, **49**, pp.395-402 (1986).

31. Wang, J., Sukhorukov, V.L., Djuzenova, C.S., Zimmermann, U., Müller, T. and Fuhr, G., "Electrorotational spectra of protoplasts generated from the giant marine alga valonia utricularis", *Protoplasma,* **196**, pp.123-134 (1997).

32. Gisma, J., Glaser, R., and Fuhr, G., "Interpretation of electroroation of protoplasts", *Studia Biophysica*, **109**, pp.5-14 (1985).

33. Kaler, K.V.I.S. and R. Johnston, "Spinning response of yeast cells to rotating electric fields", *J. Biol. Phys.*, **13**, pp.69-73 (1985).

34. Sheng, Y., Kaler, K.V.I.S., Hriskevich, B. and Paul, R., "An automated electro-rotation measurement system", *15th Annual International Conference IEEE Engineering in Medicine and Biology Society*, San Diego, USA, October 28-31 (1993).

35. Huang, Y., Holzel, R., Pethig, R. and Wang, X., "Difference in the Ac electrodynamics of viable and non-viable yeast cells determined through combined dielectrophoresis and electrorotation studies", *Phys. Med. Biol.*, **37 (7)**, pp.1499-1517 (1992).

36. Wang, X., Huang, Y., Hölzel, R., Burt, J.P.H. and Pethig, R., "Theoretical and experimental investigations of the interdependence of the dielectric, dielectrophoretic and electrorotational behaviour of colloidal particles", *J. Phys. D: Appl. Phys.*, **26**, pp.312-322 (1993).

37. Lovelace, R.V.E., Stout, D.G. and Steponkus, P.I., "Protoplasts rotation in a rotating electric field: The influence of cold acclimation", *J. Membrane Biol.*, **82**, pp.157 (1984).

38. Hölzel, R. and Lamprecht, I., "Dielectric properties of yeast cells as determined by electrorotation", *Biochimica et Biophysica Acta.*, **1104**, pp.195-200 (1992).

39. Holzapfel, J., Vienken, J. and Zimmermann, U., "Rotation of cells in an alternating electric field: Theory and experimental proof", *J. Membrane Biol.*, **67**, pp.13-26 (1982).

40. Zimmermann, U. and Neil, G.A., *Electromanipulation of cells,* CRC Press, New York (1996).

41. Jeltsch, E. and Zimmermann, U., " Particles in a homogenous electrical field: a model for the electrical breakdown of living cells in a coulter counter" *Bioelectrochem. Bioenerg.*, **6**, pp.349-384 (1979).

42. Tucu, I. and Lucaciu, C.M., "Electro-rotation: A spherical shell model", *J. Phys. A: Math. Gen.*, **22**, pp.995-1003 (1989).

43. O'Konski, C.T., "Electric properties of macromolecules. Theory of ionic polarization in polyelectrolytes", *J. Phys. Chem.*, **64**, pp.605 (1960).

44. Schwarz, G.J., "A theory of the low-frequency dielectric dispersion of colloidal particles in electrolyte solution", *J. Phys. Chem.*, **66**, pp.2636 –2642 (1962).

45. Dukhin, S.S. and Shilov, V.N., *Dielectric phenomena and the double layer in dispersed systems and polyelectrolytes*, halted: Jerusalem (1974).

46. Paul, R., Kaler, K.V.I.S. and Jones, T.B., "A nonequilibrium statistical mechanical calculation of the surface conductance of the electrical double layer of biological cells and its application to dielectrophoresis", *J. Phys. Chem.*, **97**, pp.4745-4755 (1993).

47. Atkins, P.W., *Physical Chemistry*, fifth edition, W.H. Freeman and company, New York, (1994).

48. Grant, E.H., Sheppard, R.J. and South, G.P., *Dielectric behaviour of biological molecules in solution*, Clarendon Press, Oxford, (1978).

49. Foster, K.R., Sauer, F.A. and Schwan, H.P., "Electro-rotation and levitation of cells and colloidal particles", *Biophys. J.*, **63**, pp.180-190 (1992).

50. Pastushenko, V.Ph., Kuzjmin, P.I. and Chizmadzhev, Yu.A., "Dielectrophoresis and electro-rotation- a unified theory of spherically symmetrical cells", *Studia Biophysica*, **110**, pp.51-57 (1985).

51. Chizmadzhev, Yu.A., Kuzmin, P.I. and Pastushenko, V.Ph., "Theory of the dielectrophoresis of vesicles and cells", *Biological Membranes* (USSR), **2**, pp.1147-1161 (1985).

52. Paddison, S.J., *Nonlinearities in Biodielectrics*, Ph.D. Thesis, The University of Calgary, Calgary (1996).

53. Schurr, J.M., "On the theory of the dielectric dispersion of spherical colloidal particles in electrolyte solution", *J. Phys. Chem.* **68 (9)**, pp.2407-2413 (1964).

54. Fixman, M.J., " Charged macromolecules in external fields", *J. Chem. Phys.*, **72**, pp.5177 (1980).

55. Fixman, M.J., "In double layer approximations for electrophoresis and electric response", *J. Chem. Phys.*, **78**, pp.1483 (1983).

56. Chew, W.C. and Sen, P.N., "Potential of a sphere in an ionic solution in thin double layer approximations", *J. Chem. Phys.*, **77**, pp.2042 (1982).

57. Chew, W.C., , *J. Chem. Phys.*, **81**, pp.4541 (1984).

58. Grosse, C. and Foster, K.R., "Permittivity of a suspension of charged spherical particles in electrolyte solution", *J. Phys. Chem.*, **91**, pp.3073-3076 (1987).

59. Grosse, C., "I. Permittivity of a suspension of charged spherical particles in electrolyte solution. 2. Influence of the surface conductivity and asymmetry of the

electrolyte on the low-and high-frequency relaxations", *J. Phys. Chem.*, **92**, pp.3905-3910 (1988).

60. Sheng, Y., *Electrorotation studies on protoplasts*, M.Sc. Thesis, The University of Calgary, Calgary (1995).

61. Asashima, M., Malacinski, G.M. and Smith, S.C., "Surgical manipulation of embryos" in *Developmental biology of the Axolotl*, Armstrong, J.B. and Malacinski, G.M., Oxford University Press, New York, pp.256 (1989).

62. Deuchar, E.M., *Xenopus: The South African Clawed Frog*, John Wiley & Sons, London, (1975).

63. Jones, T.B., *Electromechanics of particles*, Cambridge University Press, New York, (1995).

64. Warner, A.E., "The electrical properties of the ectoderm in the amphibian embryo during induction and early development of the nervous system", *J. Physiol.*, **235**, pp.267-286 (1973).

65. Schwan, H.P., "Dielectric properties of cells and tissues" in *Interactions between electromagnetic fields and cells*, Chiabrera, A., Nicolini, C. and Schwan, H.P., Plenum Press, New York, pp.75 (1985).

66. Metcalf, M.E.M. and Borgens R., "Weak applied voltages interfere with amphibian morphogenesis and pattern", *The Journal of Experimental Zoology*, **268**, pp.323-338 (1994).

67. Nieuwkoop, P.D., Bjõrklund, N.K. and Gordon, R., "Surface contraction and expansion waves correlated with differentiation in Axolotl embryos. In contrast to

Urodeles, the anuran xenopus laevis does not show furrowing surface contraction waves", *Int. J. Dev. Biol.*, **40**, pp.661-664 (1996).

68. Jackson, J.D., *Classical Electrodynamics*, 2nd edition, Wiley, New York, (1975).

69. Smith, H.M., "Discovery of the Axolotl and its early history in biological research" in *Developmental biology of the Axolotl*, Armstrong, J.B. and Malacinski, G.M., Oxford University Press, New York, pp.3 (1989).

70. Gordon, R. and Brodland, G.W., "Neurulation" in *Developmental biology of the Axolotl*, Armstrong, J.B. and Malacinski, G.M., Oxford University Press, New York, pp.62 (1989).

71. Bordzilovskaya, N.P., Dettlaff, Duhon, S.T. and Malacinski, G.M., "Developmental-stage series of Axolotl embryos" in *Developmental biology of the Axolotl*, Armstrong, J.B. and Malacinski, G.M., Oxford University Press, pp.201 (1989).

APPENDIX A

BIOLOGY OF AXOLOTL EMBRYOS

Axolotls, classified under Urodela order of amphibians, have become one of the most widely used experimental subjects in the world. Since 1865, when a flood of publications on the Axolotl began in France, several thousand scientific and numerous popular articles have been written on Axolotls [69]. In many laboratories, Axolotl animals are maintained in aerated large containers of treated water (or a small aquarium for a single animal) at $18^0C - 20^0C$.

Axolotl embryos have many advantages when compared with other amphibians. For example the eggs are relatively large (about 2 mm in diameter) and the ectoderm is a monolayer of cells [70], allowing the interior to be easily observed and models approximating the simple structure to be constructed. Moreover, Axolotl embryos are highly pigmented with the amount of pigmentation varying from one cell to another thus enabling the cell movements to be followed without the use of dyes. In addition, Axolotl eggs have a slow developmental rate, which can be also controlled since they can tolerate a wide temperature range ($4^0C - 25^0C$). As a consequence, it is easy to work with several embryos from the same spawning or allow them to arrive to some pre-determined convenient developmental stage.

Developmental Stages of Axolotl Embryos:

Bordzilovskaya and Dettlaff [71] divided the development of Axolotl into 43 stages, based on external morphology. The developmental-stage series they published, and adopted for identifying stages in the present thesis, is shown at the end of this appendix. A jelly coat encapsulates an Axolotl egg when it is freshly laid. An Axolotl

zygote (fertilized egg) can be seen as a sphere divided into two hemispheres: the animal pole (the upper part) is pigmented while the vegetal pole is not pigmented. Cleavage, when the zygote undergoes a series of five or six divisions into 2, 4, 8, 16 etc cells or blastomeres, is the first phase of development. More divisions continue to occur during which the embryo acquires an internal cavity and is then called a blastula [62].

The appearance of first signs of a dorsal groove, known as blastopore, marks the beginning of gastrulation (stages 10 – 13). Gastrulation is considered the first major morphological event to occur during amphibian development. This process starts when a large number of cells migrate below the surface to form two inner layers, the mesoderm and endoderm, while the cells which remain outside spread to cover the whole surface of the embryo, forming the ectoderm [62]. Invagination of mesoderm cells at the blastopore is another phenomenon that occurs during gastrulation. It is suggested that the migration of mesoderm cells by contact guidance is controlled by the extracellular fibrils on the inner surface of the ectodermal layer of the Axolotl gastrulae.

Neurulation involves differentiation of the ectoderm into epidermis and neuroepithelium, which are tissues that ultimately form the skin and central nervous system, respectively. This phase begins at stage 14 when a neural plate starts to form in the dorsal ectoderm. The plate rolls up at its sides to form the neural tube [62]. The margins of the neural tube are completely fused at stage 21 (end of neurulation). After that, most of the features become visible and the beginning of muscular movements cause the embryo to break out of its jelly capsule and become a hatched larva. The whole process, from fertilization to hatching, takes about 265 hours at 20^0C.

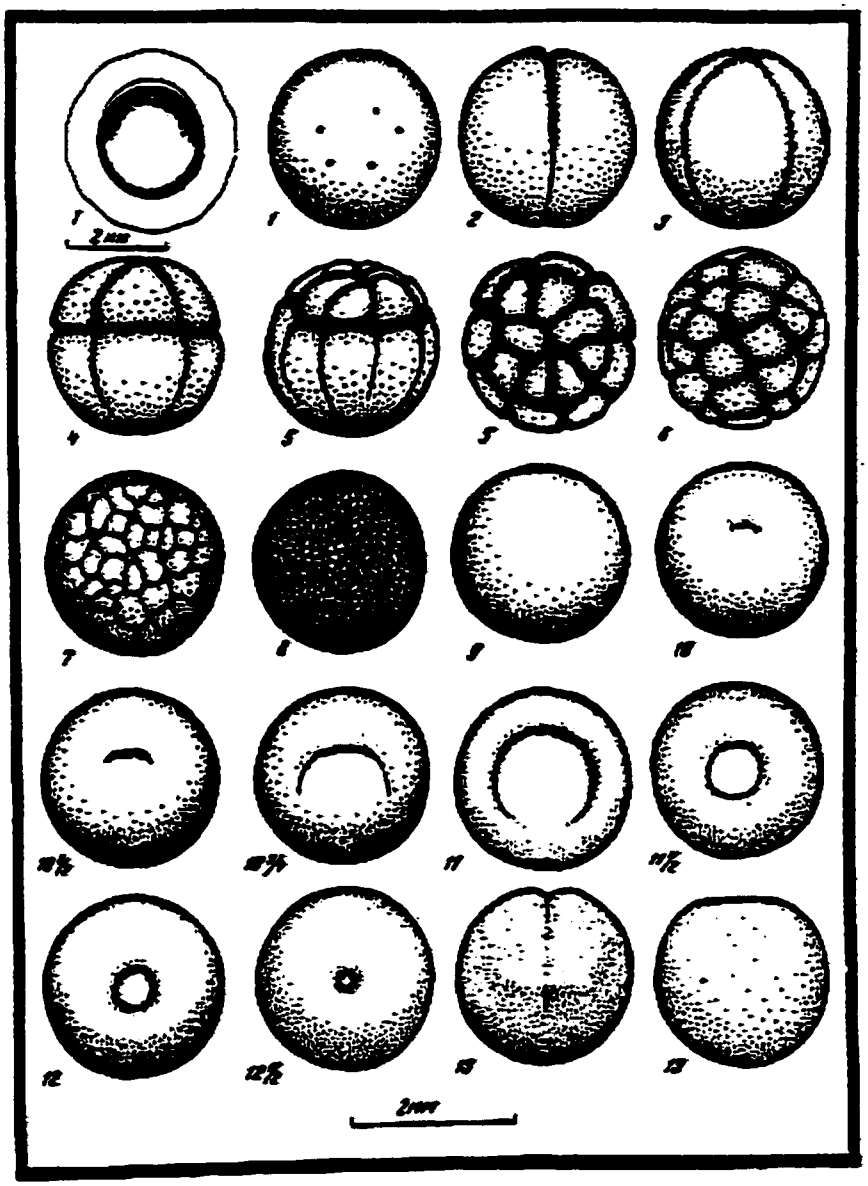

Developmental-Stage Series of Axolotl Embryos

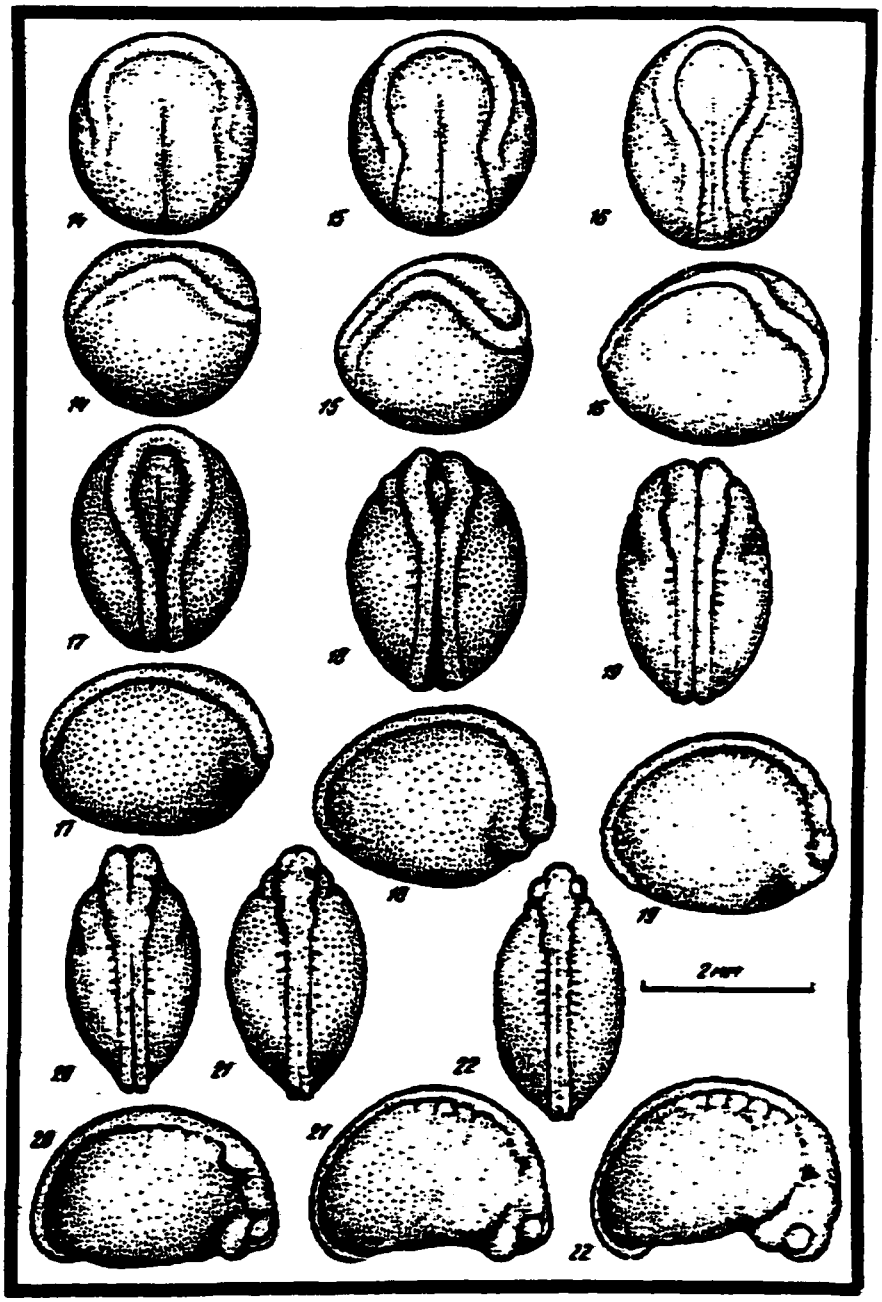

Developmental-Stage Series of Axolotl Embryos (cont'd)

APPENDIX B

SOLUTION OF LAPLACE EQUATION AND SPHERICAL HARMONICS

As the solution of Laplace equation is fundamental to the theoretical model presented in this thesis (chapter 5), it is convenient to familiarize the reader with the solution along with the associated spherical harmonics.

The study of dielectrics requires the knowledge of the distribution of the electric potential in a number of polarized regions in a system. It is simpler to take the potential as a function of r,θ,ϕ and then eliminate ϕ, the azimuthal angle, at the end. The Laplace equation:

$$\nabla^2\Psi(r,\theta,\phi)=0 \tag{B.1}$$

has a general solution:

$$\Psi(r,\theta,\phi)=\sum_{n=0}^{\infty}\sum_{m=-n}^{n}\left[A_{nm}r^{n}+B_{nm}r^{-(n+1)}\right]Y_{nm}(\theta,\phi) \tag{B.2}$$

Here $Y_{nm}(\theta,\phi)$ is the spherical harmonics given by:

$$Y_{nm}(\theta,\phi)=\sqrt{\frac{2n+1(n-m)!}{4\pi(n+m)!}}P_n^m(Cos\theta)e^{im\phi} \tag{B.3}$$

$P_n^m(Cos\theta)$ is the Associated Legendre Polynomial. The coefficients A_{nm} and B_{nm} are determined from the boundary conditions.

Using equation (B.3), we write the explicit forms of the various spherical harmonics required in this work:

$$Y^{*}_{1,-1}(\alpha,\beta) = e^{i\beta}\sqrt{\frac{3}{8\pi}}Sin\alpha \tag{B.4}$$

$$Y^{*}_{1,0}(\alpha,\beta) = \sqrt{\frac{3}{4\pi}}Cos\alpha \tag{B.5}$$

$$Y^{*}_{1,1}(\alpha,\beta) = -e^{-i\beta}\sqrt{\frac{3}{8\pi}}Sin\alpha \tag{B.6}$$

$$Y^{*}_{1,0}(\pi-\alpha,\pi+\beta) = -\sqrt{\frac{3}{4\pi}}Cos\alpha \tag{B.7}$$

$$Y^{*}_{1,-1}(\pi-\alpha,\pi+\beta) = -e^{i\beta}\sqrt{\frac{3}{8\pi}}Sin\alpha \tag{B.8}$$

$$Y^{*}_{1,1}(\pi-\alpha,\pi+\beta) = e^{-i\beta}\sqrt{\frac{3}{8\pi}}Sin\alpha \tag{B.9}$$

Also, we assume the electric field is described by:

$$E^{*}_{11} = -\frac{4}{3}\pi E_0 e^{-i\varphi}\sqrt{\frac{3}{8\pi}}Sin\gamma \tag{B.10}$$

$$E^{*}_{10} = \frac{4}{3}\pi E_0 \sqrt{\frac{3}{4\pi}} Cos\gamma \qquad \text{(B.11)}$$

$$E^{*}_{1-1} = \frac{4}{3}\pi E_0 e^{i\varphi} \sqrt{\frac{3}{8\pi}} Sin\gamma \qquad \text{(B.12)}$$

For negative m values, the following identity was used:

$$Y_{l,-m}(\theta,\phi) = (-1)^{m} Y^{*}_{lm}(\theta,\phi) \qquad \text{(B.13)}$$